Elsevier Editorial System(tm) for Geomorphology
Manuscript Draft

Manuscript Number:

Title: Bedform genesis in bedrock substrates: insights into formative processes from a new experimental approach and the importance of suspension-dominated abrasion

Article Type: Research Paper

Keywords: physical modelling; bedrock bedforms; bedrock erosion; suspension-dominated abrasion.

Corresponding Author: Dr. Daowei Yin,

Corresponding Author's Institution: East China Normal University

First Author: Daowei Yin

Order of Authors: Daowei Yin; Jeff Peakall, Dr.; Dan Parsons, Dr.; Zhongyuan Chen, Dr.; Heather Macdonald, Dr.; Paul Wignall, Dr.; Jim Best, Dr.

Abstract: Bedrock channels are common in the natural environment and bedrock channel erosion sets the pace of denudation in many of the world's river catchments. However, there have been very few investigations that concern either bedrock bedform genesis or bedrock channel abrasion processes. Field based analysis of sculptured forms within bedrock channels has been restricted notably by the slow rate of bedform development in such environments. Few flume-scale experiments have been conducted that attempt to simulate the genesis of sculpted bedforms in bedrock channels. This study demonstrates that optimisation of clay beds through successfully matching clay strength enables the development of features analogous to bedrock river channel bedforms. Three sets of sediment-laden experiments were carried out using hard, medium and soft clay beds, respectively. A suite of erosive bedforms, including potholes, flutes, and furrows developed on all experimental beds. All observed erosional features have clear equivalents to those observed in natural bedrock rivers. This work further demonstrates that in the absence of suspended sediment, fluid flow cannot induce erosion in cohesive or bedrock substrates. Basal shear strength was a significant factor for the genesis of different types of simulated bedrock bedforms in our experiments. Lastly this work illustrates that abrasion by suspended sediments is the only driving force necessary for the formation of these bedrock bedforms, because the erosional features were produced in the absence of bed load abrasion, plucking, cavitation and dissolution.

Suggested Reviewers: Paul Carling Dr.
Emeritus Professor in Physical Geography, Geography and Environment, University of Southampton
P.A.Carling@soton.ac.uk

Michael Lamb Dr.
Professor of Geology, Division of Geological and Planetary Sciences, California Institute of Technology
mpl@gps.caltech.edu

Rebecca Hodge Dr.
Lecturer, Department of Geography, Durham University
rebecca.hodge@durham.ac.uk

State Key Laboratory of Coastal and Estuarine Research
East China Normal University
Shanghai, 200020
China
30, June, 2015

Dear Editor:

Please find enclosed a manuscript entitled: “Bedform genesis in bedrock substrates: insights into formative processes from a new experimental approach and the importance of suspension-dominated abrasion” which I am submitting for exclusive consideration for publication in Geomorphology.

The paper demonstrates the formation of a variety of bedrock bedforms under the effect of suspension-dominated abrasion through physical laboratory modelling for the first time. As such this paper will be of interest to a broad readership including those interested in fluvial processes and landscape changes.

Knowledgeable referees for this paper might include:

- Paul Carling: Professor in Physical Geography. P.A.Carling@soton.ac.uk;
- Michael Lamb: Professor of Geology. mpl@gps.caltech.edu;
- Rebecca Hodge: Lecturer, Department of Geography, Durham University. rebecca.hodge@durham.ac.uk

I confirm that this paper has not been submitted elsewhere or published. Thank you for your consideration of our work. We look forward to an editorial decision.

Sincerely,

Daowei Yin

Highlights

- Flume-scale experiments using modelling clay produced more than 30 kinds of erosional features analogous to natural bedrock sculpted forms.
- Results showed erosive bedforms were developed under the sole effect of abrasion without cavitation, dissolution, corrosion or plucking.
- The experimental surfaces and the erosional bedforms were the result of suspension driven abrasion rather than bed load driven saltation dominated abrasion.
- Basal shear strength was a significant factor for the variety of bedrock bedforms in our experiments.

Bedform genesis in bedrock substrates: insights into formative processes from a new experimental approach and the importance of suspension-dominated abrasion

Daowei Yin[1,2]*

[1] School of Earth and Environment, University of Leeds, Leeds, UK;

[2] State Key Laboratory of Coastal and Estuarine Research, East China Normal University, Shanghai 200062, China. Nicholas_t_yin@hotmail.com;

* Corresponding author

Jeff Peakall[1]

[1] School of Earth and Environment, University of Leeds, Leeds, UK. J.Peakall@leeds.ac.uk;

Dan Parsons[3]

[3] Department of Geography, Environment and Earth Science, University of Hull, Hull, UK. d.parsons@hull.ac.uk;

Zhongyuan Chen[2]

[2] State Key Laboratory of Coastal and Estuarine Research, East China Normal University, Shanghai 200062, China. z.chen@ecnu.edu.cn;

Heather Macdonald[1,4]

[1] School of Earth and Environment, University of Leeds, Leeds, UK;

[4] ExxonMobil Exploration Company, 222 Benmar Drive, Houston, Texas 77060, USA. h.macdonald@see.leeds.ac.uk;

Paul Wignall[1]

[1] School of Earth and Environment, University of Leeds, Leeds, UK. P.B.Wignall@leeds.ac.uk;

Jim Best[5]

[5] Departments of Geology, Geography and GIS, Mechanical Science and Engineering and Ven Te Chow Hydrosystems Laboratory, University of Illinois, Urbana-Champaign, IL 61801, USA. jimbest@illinois.edu.

Abstract

Bedrock channels are common in the natural environment and bedrock channel erosion sets the pace of denudation in many of the world's river catchments. However, there have been very few investigations that concern either bedrock bedform genesis or bedrock channel abrasion processes. Field based analysis of sculptured forms within bedrock channels has been restricted notably by the slow rate of bedform development in such environments. Few flume-scale experiments have been conducted that attempt to simulate the genesis of sculpted bedforms in bedrock channels. This study demonstrates that optimisation of clay beds through successfully matching clay strength enables the development of features analogous to bedrock river channel bedforms. Three sets of sediment-laden experiments were carried out using hard, medium and soft clay beds, respectively. A suite of erosive bedforms, including potholes, flutes, and furrows developed on all experimental beds. All observed erosional features have clear equivalents to those observed in natural bedrock rivers. This work further demonstrates that in the absence of suspended sediment, fluid flow cannot induce erosion in cohesive or bedrock substrates. Basal shear strength was a significant factor for the genesis of different types of simulated bedrock bedforms in our experiments. Lastly this work illustrates that abrasion by suspended sediments is the only driving force necessary for the formation of these bedrock bedforms, because the erosional features were produced in the absence of bed load abrasion, plucking, cavitation and dissolution.

1. Introduction

Bedrock rivers exhibit a diverse array of erosional forms, that in turn influence flow fields and sediment dynamics (Richardson and Carling, 2005). The genesis and formative processes of these erosional features is poorly understood, and remains an area where there is a major knowledge gap (Lamb et al., 2015). This is largely because field studies are limited by the slow rate of development of erosion within bedrock substrates, and by the difficulty and danger of attempting to measure processes during infrequent high magnitude flow events (Lamb et al., 2015). Physical experiments offer the opportunity to examine processes at much faster development rates, and under controlled conditions (Peakall et al., 1996; Lamb et al., 2015). However, there have been relatively few studies of erosive bedforms in substrates analogous to those observed in bedrock rivers (Shepherd and Schumm, 1974; Wohl and Ikeda, 1997; Carter and Anderson, 2006; Johnson and Whipple, 2007; Johnson and

Whipple, 2010; Wilson et al., 2013; Wilson and Lave, 2014). Furthermore, these studies have only reproduced a small number of the features identified in natural channels (Richardson and Carling, 2005). Model studies on actual rock substrates have been restricted to forming upstream facing convex surfaces (Wilson et al., 2013; Wilson and Lave, 2014). In contrast, studies utilising artificial substrates exhibit a wider range of features, with those on concrete (Carter and Anderson, 2006; Johnson and Whipple, 2007; Johnson and Whipple, 2010) and mixed sand/mud substrates (Shepherd and Schumm, 1974; Wohl and Ikeda, 1997) producing longitudinal grooves, potholes, and furrows. Even in these cases, experiments with initially broad erosion surfaces are dominated by longitudinal grooves that over time form 'emergent channel geometries' (Shepherd and Schumm, 1974; Wohl and Ikeda, 1997; Finnegan et al., 2007; Johnson and Whipple, 2007; Johnson and Whipple, 2010; Lamb et al., 2015). Consequently, despite these advances, experiments have failed to produce the wide variety of bedforms observed in natural systems, and the broad spatial distribution of these erosive features. In turn, this raises questions as to the nature of the experimental conditions and physical processes required to reproduce many of these bedrock bedforms. Here, we utilise compacted clay substrates to reproduce most of the observed features present in bedrock rivers (c.f. Richardson and Carling (2005)). The nature of the formative conditions are discussed and compared to existing physical modelling and field studies.

1.1. Previous erosional experiments with clay beds

Although clay substrates have been used to study erosional bedforms in physical experiments, these studies produced features such as flutes and longitudinal grooves that have been compared to natural erosion in cohesive muddy substrates such as deep-sea muds and river floodplains (e.g., Dzulynski and Sanders, 1962; Dzulynski and Walton, 1963; Dzulynski, 1965, 1996; Allen, 1969,1971). Furthermore, the applicability of these mud-rich cohesive sediments to bedrock rivers has been questioned (e.g., Lamb et al. (2015)) because of the absence of brittle fracturing that typically occurs in bedrock erosion (Engel, 1976). The majority of experiments that have been undertaken on weak muddy substrates, typically used beds formed from *in situ* settling of clays in water for periods of hours to days (e.g., Dzulynski and Walton, 1963; Dzulynski, 1965, 1996; Allen, 1969, 1971), producing a range of features such as flutes and groove marks. In contrast, there has been very little work on firm or hard mud beds. Allen (1971) undertook a series of 13 experiments in a Perspex pipe, where particulate-flows eroded beds of kaolin-based modelling clay, producing flute like features. Run times were between 27 and 74 minutes, although these experiments could not be continued beyond these timescales as a series of bed waves developed (Allen, 1971).

Dzulynski and Sanders (1962) also used modelling clay to examine tool marks, but these experiments were undertaken by rolling objects by hand across subaerially exposed clay. Whilst these experiments on weak and firm clay beds have demonstrated a range of erosive features, there is an absence of quantitative data on substrate strength, such as the shear strength, and on flow properties such as basal shear stress, with which to explore the boundary conditions of such erosive features. The experiments presented here revisit the utility of clay substrates for modelling bedrock erosion, but under conditions where the substrate strength and basal shear stress are quantified, and we examine the development of erosive features in the absence of brittle fracturing.

1.2. Erosive mechanisms in bedrock substrates

The major erosional mechanisms postulated to control the morphology and genesis of bedrock channels are: (1) abrasion (Hancock et al., 1998; Wohl, 1998; Whipple et al., 2000a; Sklar and Dietrich, 2001; Sklar and Dietrich, 2004; Johnson and Whipple, 2007; Wilson et al., 2013; Wilson and Lave, 2014); (2) plucking (Baker, 1973; Hancock et al., 1998; Whipple et al., 2000a; Whipple et al., 2000b; Lamb and Fonstad, 2010); (3) cavitation (Baker, 1974; Wohl, 1992; Baker and Kale, 1998; Hancock et al., 1998; Wohl, 1998; Whipple et al., 2000a; Whipple et al., 2000b); and (4) dissolution or corrosion (Wohl, 1992; Wohl, 1998; Whipple et al., 2000a). Of these, abrasion and plucking are considered the most important processes, with plucking effective when rocks are fractured and exhibit discontinuities, whilst abrasion is thought to dominate in massive rock with weak jointing (Hancock et al., 1998; Whipple et al., 2000a; Lamb and Fonstad, 2010). Abrasion can occur as a result of either saltating bed load or as suspended-load, with debate on the relative efficacy of these two modes in bedrock rivers (Hancock et al., 1998; Whipple et al., 2000a). Evidence for the importance of cavitation in the field and experiments is lacking, although theoretically it is thought to be a plausible contributing factor (Whipple et al., 2000a; Carling et al., 2009). Weathering of bedrock through corrosion may also be important, but has been little studied using experiments (Lamb and Fonstad, 2010).

2. Methodology

A series of four experimental runs were undertaken to examine the nature of erosion in clay beds by open channel flow, three containing a particulate load of fine-grained sand and one without particulate load (clear water). Air-dried modelling clay was used as the substrate, with the initial undrained shear strength of the clay beds adjusted between runs through pre-soaking of the clay bed.

Experimental setup

An 8.75 m long, tilting, recirculating hydraulic slurry flume (0.30 m wide by 0.30 m deep) was used for the experiments (Fig. 1). The flume contained a false floor into which a tray (0.90 m long and 0.075 m deep) containing clay could be inserted, such that the upper surface of the clay-bed was flush with the false floor (Fig. 1). The water depth was set to 0.14 m above the clay bed in all experiments, and uniform flow was obtained by adjusting the flume slope to 0.005. An array of ten 4 MHz ultrasonic Doppler velocimetry probes (UDVP; (Best et al., 2001)) were positioned downstream of the clay bed, pointing upstream, with the ends of the transducers positioned level with the end of the clay bed (Fig. 1). The UDVP collected data for 99 seconds at a temporal resolution of 8 Hz; the operating parameters for the UDVP are shown in Table 1. The UDVP probes enabled flow velocity profiles, initial basal shear stress (Exp. 1: $\tau \approx 3.10$ Nm^{-2}; Exp. 2: $\tau \approx 4.85$ Nm^{-2}; no data for Exp. 3 but of similar order to experiments 1 and 2), and mean flow velocity (V_{mean} = 0.75-0.81 ms^{-1}), to be measured above the clay bed. A further experiment (Exp. 4) was run for 12 hours without a sediment load or bed defects, with an undrained shear strength of 10.5 kPa, initial basal shear stress of 3.10 Nm^{-2} and flow velocity of ~0.81 ms^{-1}. Water temperature during the experiments varied between 8-10°C.

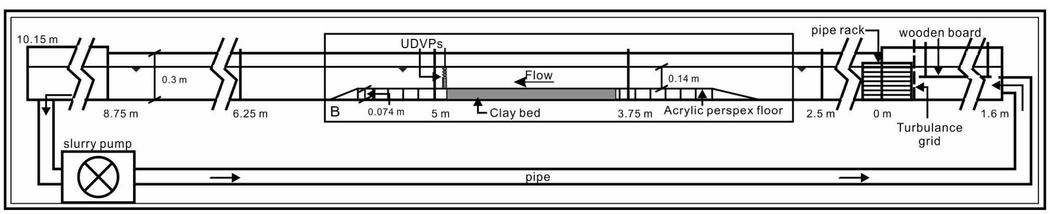

Figure 1. Schematic drawing of the experimental setup of the hydraulic slurry flume. The dark area represents the clay bed with a tray that was lowered into position so that the top surface of the clay bed was flush with the surrounding false floor.

Table 1. Parameters for the UDVP used in the presented experiments

Ultrasonic frequency	Bin Width	Bin distance	Measurement window	Number of bins	Multiplexing time delay	Number of profiles per transducer	Ultrasound velocity	Transducer diameter	Bins for analysis
4 MHz	1.48 mm	0.74 mm	5-101.2 mm	128	15 ms	500	1480 ms^{-1}	8 mm	31-38

Clay preparation and undrained shear strength measurement

Air-dried modelling clay (Potter's Scola Clay) was used as the substrate and consisted primarily of illite-smectite, kaolinite and quartz (Table 2). The pre-soaking time was altered to adjust the initial undrained shear strength of the substrate from 10.5 kPa (Exp. 1), through 7.5 kPa (Exp. 2) to 5.5 kPa (Exp. 3) (Fig. 2) - referred to herein as hard, medium and soft. Shear strength was measured using a hand shear vane meter with a four-blade vane (25.4 mm wide by 50.8 mm deep). After soaking to the required strength, the clay was placed in a tray and inserted into the flume. In order to ensure the original bed surface was flat the clay surface was smoothed by hand using a metal board to the same level as the surrounding Perspex floor.

Table 2 X-ray diffraction analysis of modelling clay used in the experiments

	Quartz	Illite-smectite	Kaolinite	Hematite
Chemical composition (%)	35.3	39.1	21.1	4.5

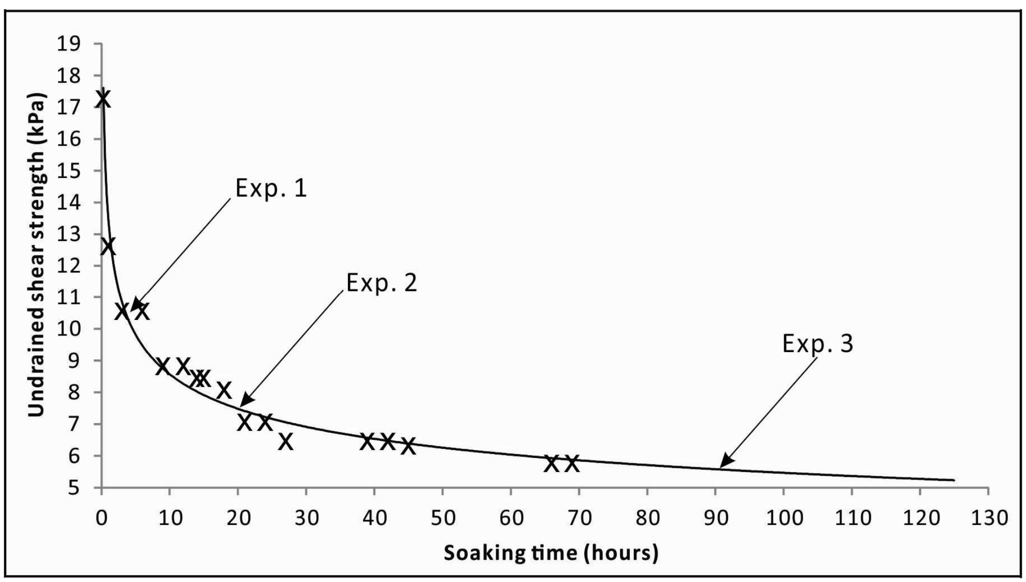

Figure 2 Variation in undrained shear strength with soaking time. Positions of the initial undrained shear strengths are shown for each experiment; Exp. 1: Hard: 10.5 kPa; Exp. 2: Medium: 7.5 kPa; Exp. 3: Soft: 5.5 kPa.

Experimental conditions

Experiments were initiated with both smooth clay beds (Exps. 2 and 3) and with a number of circular bed defects (Exp. 1; Fig. 3). The defects consisted of five large holes 2.4

cm in diameter and 0.3 cm in depth, two medium-sized hollows 0.9 cm in diameter and 0.2 cm in depth, and 2 smaller holes 0.6 cm in diameter and 0.2 cm in depth (Exp. 1; Fig. 3). Each experiment was then run until no further morphological change of the clay bed was observed, in part corresponding with the substrate beginning to be covered by sand deposited from suspension. Consequently the total run times of experiments 1-3 (hard, medium, soft) were 1680 min, 1800 min, and 1080 min respectively. The experiments were stopped periodically in order to take photographs after slowly draining the flume (e.g., Fig. 3b). These breaks in each experimental run took place at 1 and 2 hours and then every 2 hours until the end of the experiment, with an additional sampling point at 30 minutes for experiment 1. In order to rectify the distorted photographs, four straight control bars with 10 control points on each of them were distributed around the edges of the clay bed and corrections were undertaken using DxO ViewPoint software. Silica sand with a D_{10} of 82 µm, D_{50} of 143 µm, and D_{90} of 245 µm was added to the flow. In order to maintain a constant suspended sediment concentration (SSC), 1.5 kg of sand was progressively introduced every 15 minutes, thus compensating for sediment deposited in the pipework of the hydraulic flume. Sediment concentration was monitored via water samples collected at a depth of ~7 cm above the Perspex floor and ~10 cm downstream of the clay beds every 20 minutes; 95% of all SSC measurements were in the range of 0.10% to 0.20% by weight.

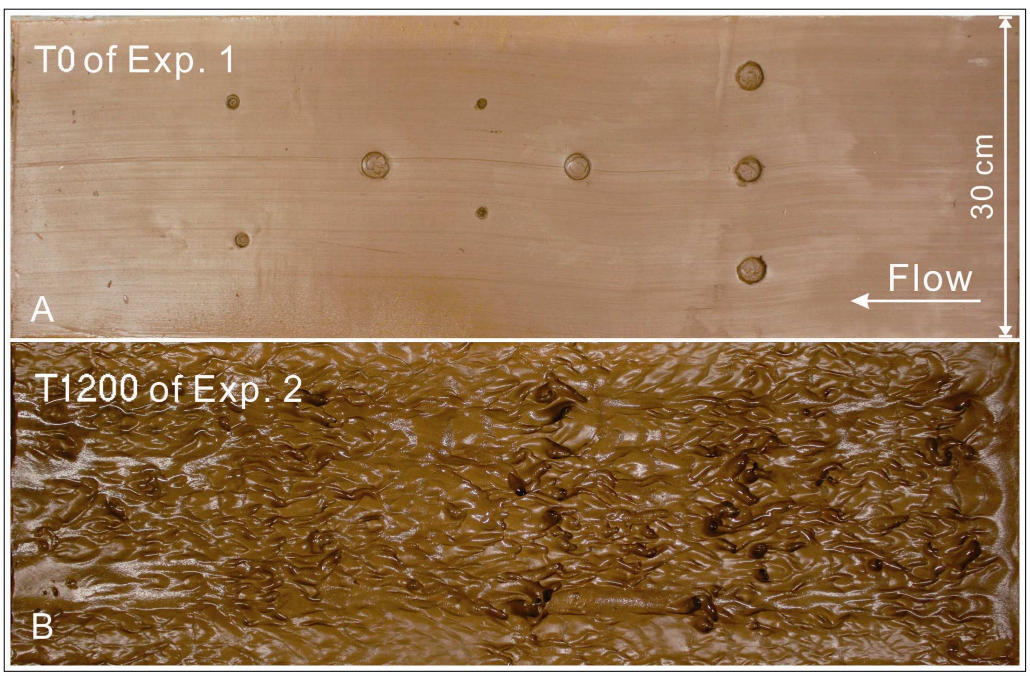

Figure 3 A: The initial experimental bed of Exp. 1: Hard, the pre-formed larger holes are 2.4 cm in diameter and 0.3 cm in depth; the medium-sized hollows are 0.9 cm in diameter and 0.2 cm in depth, and the smallest hollows are 0.6 cm in diameter and 0.2 cm in depth. B: The fully developed experimental bed of Exp. 2 after 1200 minutes run time. The initial bed of Exp. 2 was a flat bed without hollows. Flow was from right to left in both cases.

3. Results

Clear water experiment

The experiment undertaken without a sediment load or bed defects (Exp. 4) and run over 12 hours exhibited no bed erosion.

Evolution of the clay bed

The evolution and erosion rate of the clay bed differed between the three experiments with a suspended-load (Exps. 1-3) as a function of the undrained shear stress. For the hard clay bed (10.5 kPa), the bed barely altered until after 960 minutes and stopped eroding after 1440 minutes, whilst for the medium bed (7.5 kPa) bedforms initiated after 720 minutes and stopped eroding after 1320 minutes. The erosion of the softest experimental bed (5.5 kPa) began after 480 minutes and ended at 960 minutes, although this run was initiated with a series of bed defects restricting direct temporal comparison. Whilst bedform development occurred at different rates in experiments 1-3, the final forms in each showed strong similarities, with the three experiments producing an array of erosional features. Details of the most common types and geometries of these erosional features, including 4 types of potholes, 3 types of flutes, 2 types of furrows and 2 types of convex and undulating bedforms, are given below together with a comparison with natural bedrock sculpted forms.

3.1 Individual simulated erosional bedrock bedforms

Potholes

Potholes are the most common abrasion sculpture in bedrock channels (Elston, 1917; Elston, 1918; Alexander, 1932; Maxson and Campbell, 1935; Ives, 1948; Allen, 1971; Allen, 1982; Wohl, 1992; Wohl, 1993; Zen and Prestegaard, 1994; Wohl and Ikeda, 1998; Richardson and Carling, 2005) as well as the most commonly observed erosional features on the experimental clay beds. The potholes observed in the present experiments can be classified into the following categories of Richardson and Carling (2005): i) simple potholes; ii) potholes with extended exit furrows s; iii) open potholes; iv) spiral-furrowed potholes with a spiral rib ; v) spiral furrowed pothole; vi) potholes with both entry and extended exit furrows; vii) potholes with exit furrows; viii) potholes with horizontal furrows; ix) potholes with lateral external secondary furrows; x) complex potholes / convoluted potholes; and, xi) hierarchical potholes. Importantly potholes representing all 11 categories were observed. For brevity, only the details of the four most common types of pothole are described herein (Fig. 4). Extensive discussion of all the features observed is provided by Yin (2013).

Simple potholes

This kind of isolated, quasi-round pothole with a cylindrical form is common in natural bedrock channels, and was common in the current experiments (Fig. 4A1, A2. Note that dimensions of features are provided in the figures). Simple potholes could be observed on the bed as part of more complex features, or sometimes in the early stage of the experiments. These potholes typically evolved into other forms (e.g. flutes and short furrows), widening and deepening their quasi-round opening, and thus were rarely stable. The radius of the opening was usually slightly larger than that of the internal radius of its base, but the form is still regarded as approximately cylindrical. The diameter of the opening enlarged with time and extended in a specific direction, usually downstream, to form exit furrows. As a consequence, the rims of solitary potholes typically did not maintain a quasi-round geometry.

Potholes with extended exit furrows

Potholes with extended exit furrows were the most common pothole developed in the experimental beds (Fig. 4B1 to B4) The downstream ends of the exit furrows were not always closed and the lengths of the exit furrows were much bigger than the diameters of the primary potholes. The ratio of length to diameter ranges from 3.12 to 4.55 in the current case. The exit furrows usually exhibited a curved planform profile in the downstream direction with lengths more than twice as long as the widths. These features were still considered potholes because they developed from individual hollows located at the upstream end that are much deeper than the rest of the bedforms. The rims of these exit furrows were parallel, and in some cases they were closed at their downstream end (Fig. 4B1, B2). In other cases, the exit furrows were totally open at their downstream ends (Fig. 4B3, B4). Individual simple potholes could develop in time into potholes with extended exit furrows, or open potholes, if they did not connect to adjacent bedforms.

Open potholes

Open potholes are a kind of pothole that has an open end in plan view (Fig. 4C1, C2) that is almost as wide as the diameter of the primary hollow. These open potholes usually lack a lee side edge and have an entire open end whose dominant orientation is in the downstream direction. On some occasions, their upstream end rims were not closed, and they could be eroded by other marks in front of them, for example when an entry furrow developed.

Spiral-furrowed potholes with a spiral rib

On the experimental clay beds, many of the erosional marks had entry spiral ribs (e.g. (Fig. 4D1 to D3) which are widely observed in natural bedrock channels (Alexander, 1932; Ängeby, 1951; Allen, 1982; Jennings, 1983; Baker and Pickup, 1987; Wohl, 1992; Kor and Cowell, 1998; Richardson and Carling, 2005). The spiral rib is a small curved furrow extending in the upstream direction adjacent to the upstream rim of a pothole. The head of the spiral rib was usually cuspate or approximately cuspate and pointed predominantly in the upstream direction. The length and width of the spiral rib was normally far less than the primary pothole with which it was connected. The length of the spiral rib is normally no greater than 1/3 of the diameter of the primary pothole. Sometimes, near the top open rim of potholes, a secondary spiral furrow with a cuspate ridge was present within the pothole (Fig. 4D2).

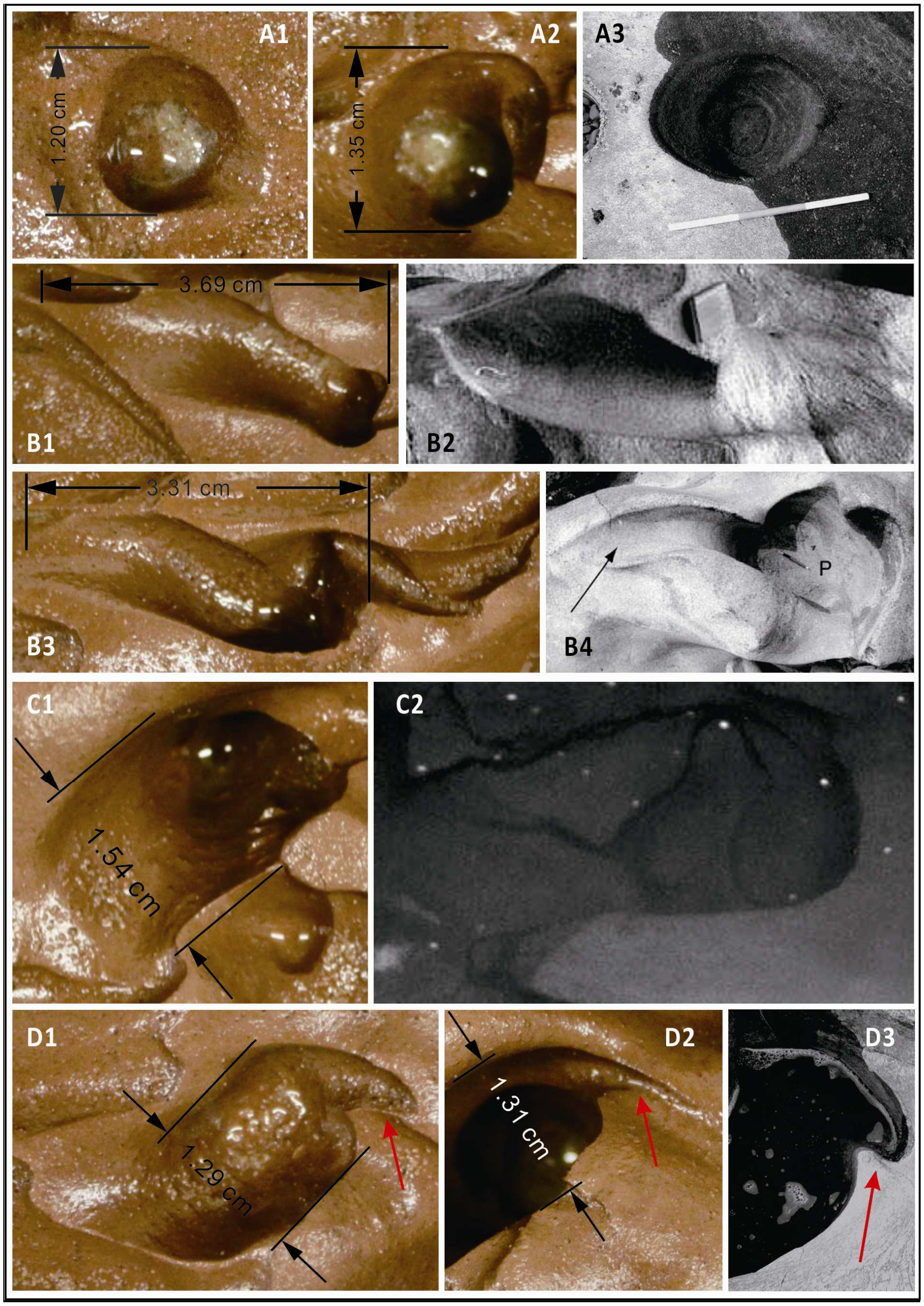

Figure 4. Morphology of potholes in the experiments and in bedrock channels. (1) Simple potholes: A1 and A2 from Exp. 2. A3 shows a simple pothole in fine-grained sandstone from the River Lune (Halton), UK (from Richardson and Carling (2005)). The scale bar in C is 0.6 m long. (2) Potholes with extended exit furrows: The exit furrows of this kind of pothole were much longer than in potholes with an entry furrow. B1 and B3 from Exp. 2. B2 and B4 are two examples from the field (from Richardson and Carling (2005)). In B2, the notebook is

0.15 m long. B3 and B4 illustrate compound potholes with extended exit furrows. See pen in B4 for scale. (3) Open potholes: C1 from Exp. 2. C2 is from the River Lune (Halton), UK. It is 1.20 m long with a diameter of 0.60 m (from Richardson and Carling (2005)). (4) Spiral-furrowed pothole with a spiral rib: The examples in D1 and D2 were observed in the central part of the bed in Exp. 2. D3 shows a natural example observed in Woolshed Creek, Australia. The pothole is ~1.5 m across in its short dimension (from Richardson and Carling (2005)). The arrow points to the spiral ribs of the potholes in D3. Flow is from right to left. A3, B2, B4, C2 and D3 are reprinted from Richardson and Carling (2005) with permission from GSA.

Longitudinal features

Besides potholes, another principal type of erosional mark in bedrock channels are longitudinal features, commonly flutes and furrows (King, 1927; Allen, 1971; Allen, 1982; Wohl, 1992; Wohl, 1993; Tinkler, 1997; Hancock et al., 1998; Richardson and Carling, 2005). Flutes and furrows are relatively shallow compared with potholes, with their depth usually being much smaller than their length (Richardson and Carling, 2005). In our experiments the average depth of the flutes was 0.82 cm compared with an average depth of 1.93 cm for the potholes (Appendix 1).

Flutes

Flutes are a common form typical of erosive bedforms in bedrock channels (Maxson and Campbell, 1935; Allen, 1971; Tinkler, 1993; Baker and Kale, 1998; Hancock et al., 1998; Whipple et al., 2000b; Richardson and Carling, 2005). The experimental approach herein produced various types of flutes that are almost identical with the flutes present in natural bedrock channels (Fig. 5).

Deep flutes

Deep flutes have been defined as those whose depth is greater than 25% of their length (Richardson and Carling, 2005). Figures 5A1 and A2 show deep flutes in our experimental substrate and natural bedrock, respectively, illustrating they are almost identical with both having a similar internal structure.

Flutes with internal secondary structure

Flutes with an internal secondary structure (Allen, 1971) formed in the experiments and show strong similarities to flutes formed in bedrock substrates (Fig. 5A1 and A2; (Richardson and Carling, 2005)). However, this type of flute was not as common as flutes with external secondary structure in the flume experiments. This may, in part, be because the scale of flutes in the present experiments was too small to contain visible smaller internal secondary structures (Fig. 5B1 and B2).

Flutes with external secondary structure

Most of the flutes in these experiments were classified as flutes with external secondary structures, formed outside the primary flutes (Fig. 5C1 to C5). Previous studies have indicated that flutes with external secondary structures may be caused by a discontinuity in the substrate (Hancock et al., 1998; Richardson and Carling, 2005). However, the clay beds used herein were well mixed and essentially homogenous, and therefore lacked any significant discontinuities. Additionally, the size of these features in the clay bed was variable, with some as large as, or only slightly smaller, than the primary flutes, whilst others were much smaller than the primary flutes. The ratio of the length of the secondary structures and the primary flutes ranges from 0.66 to 0.88 (Fig. 5C1 to C4).

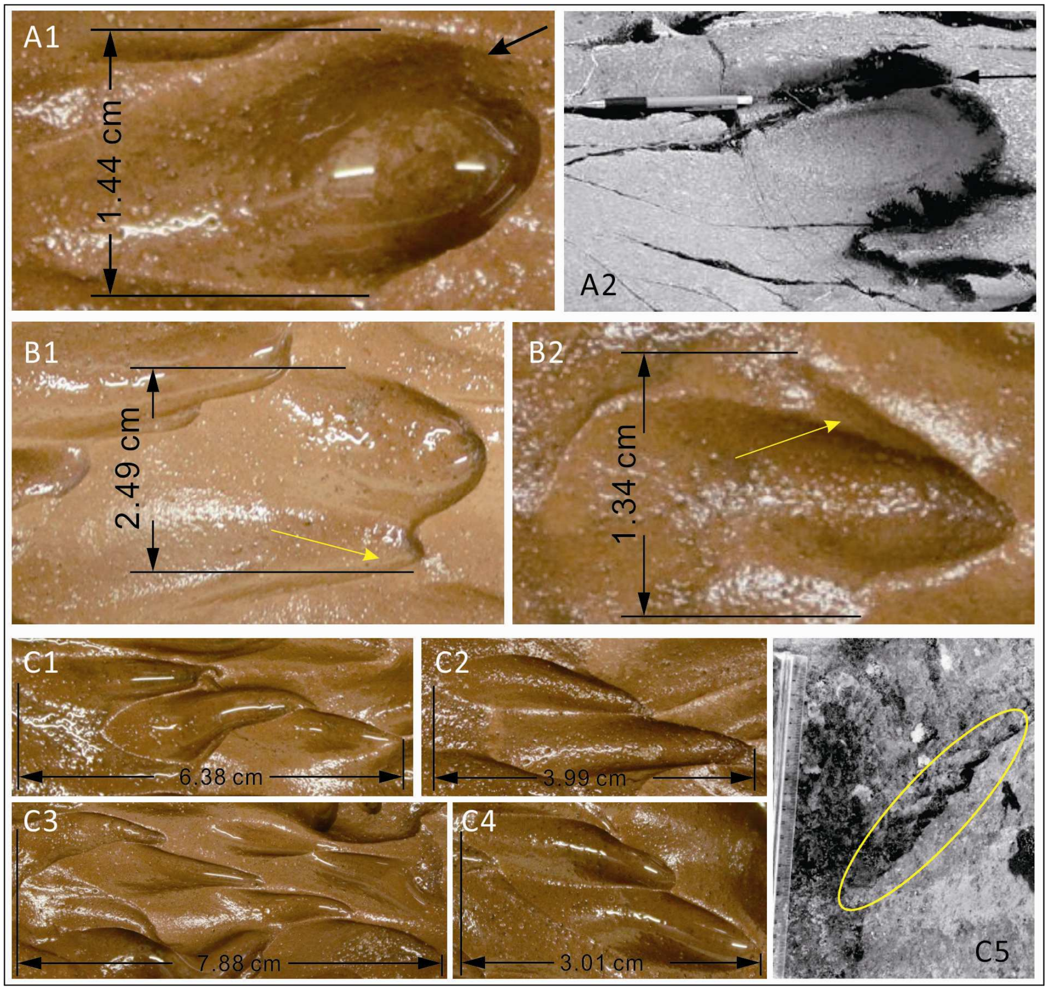

Figure 5. (1) Deep flutes: A1: deep flute in Exp. 1; A2: deep flute in the Borrow Beck, UK (from Richardson and Carling (2005), pen for scale). Both A1 and A2 contain internal secondary flutes close to their upper rims (black arrows). (2) Shallow flutes with internal secondary structure: B1 and B2 show flutes with internal secondary furrows on one side of their flanks, Exp. 2 (arrowed). (3) Flutes with external secondary structures: C1 to C4 demonstrate several rows of flutes developing in Exp. 2. Normally the first flute in a row (the rightmost flute) was regarded as the primary flute, with the remaining flutes defined as secondary. C5 shows a row of small flutes (outlined by ellipse) from the River Dee, UK; ruler in centimetres for scale (from Richardson and Carling (2005)). Flow from right to left in all cases. A2 and C5 are reprinted from Richardson and Carling (2005) with permission from GSA.

Longitudinal furrows

Furrows are also common longitudinal abrasion features in bedrock channels (Fig. 6). According to the definition of a typical furrow, the distal end should be the mirror image of its proximal end (Wohl, 1993; Wohl and Achyuthan, 2002; Richardson and Carling, 2005). The key difference between furrows and flutes is that furrows are almost symmetrical in both cross-sectional and longitudinal profile. The experimental beds demonstrated the development of most types of furrow observed in the field (Fig. 6).

Short furrows usually have closed elliptical rims in plan view (Fig. 6A1 to A4), with their depth being no more than a quarter of their length (Richardson and Carling, 2005). Typically, the average depth of these furrows was 1.37 cm and therefore not as deep as potholes (average depth: 1.93 cm), although potholes are sometimes elliptical in planform. The cross section of a short furrow is a 'U' shape, with the inner walls and bottom of the furrow usually being smooth (Richardson and Carling, 2005).

Sinuous parallel-sided furrows

The lengths of sinuous parallel-sided furrows ranged from one (1.29 cm) to more than tens of centimetres (16.22 cm) (Fig. 6B1, B2, B4), with their dominant orientation being longitudinal, with either proximal or distal ends that curved away from the flow direction, and a sinuous furrow. The rims of these furrows were mostly parallel, with their ends being either open or closed, the slope of both ends being gentle, and the rims were either round or cuspate. The walls and the bottom of these furrows were usually smooth without secondary structures or defects. Some long sinuous furrows developed from the connection of curved or sinuous short furrows, and therefore the depth of the furrows was not always uniform. Overall the morphology of these furrows was similar to field examples (Fig. 6B3).

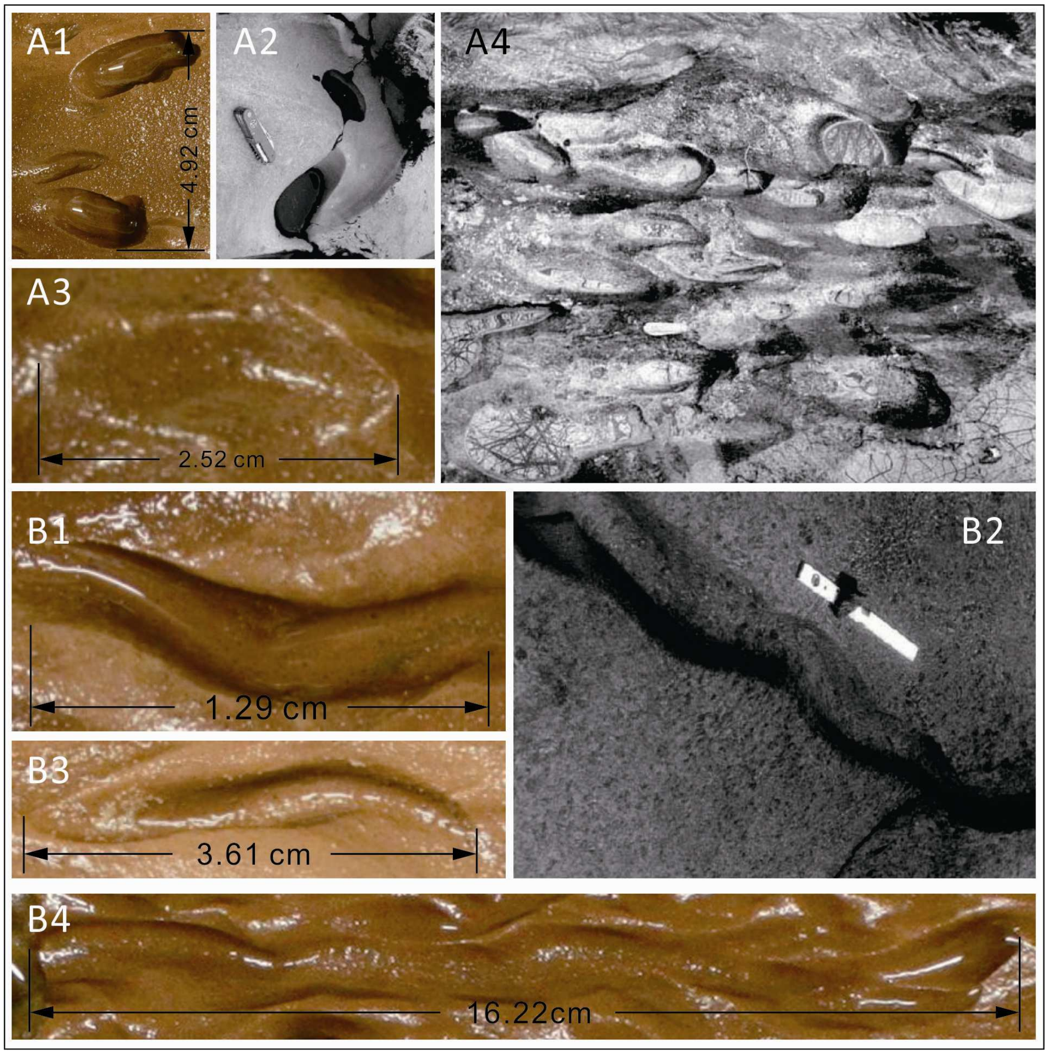

Figure 6. (1) Straight short furrows: A1 and A3 are straight short furrows in Exp. 2. A2 and A4 are field examples from the River Dee, UK; penknife in A2 and A4 (white) for scale (from Richardson and Carling (2005)). (2) Sinuous parallel-sided furrows: B1, B3 and B4: examples of features observed in Exp. 3, 2, and 1 respectively. Flow from right to left. B2 was observed in the River Lune (Halton), UK; the scale is 0.60 m long. Flow from bottom right corner to top left corner. A2, A4 and B2 are reprinted from Richardson and Carling (2005) with permission from GSA.

Convex and undulating surfaces

A number of convex and undulating surfaces also formed in the experiments, with hummocky forms being the most common type within this category (Richardson and Carling, 2005). The most common kind of hummocky form was a sharp-crested hummocky morphology, which resembles ripples and dunes found in cohesionless substrates, but possessed more obvious sharp crests (Fig. 7A1 to A3). This morphology has led to these features being termed pseudo-ripples and pseudo-dunes (Ängeby, 1951; Hancock et al., 1998; Whipple et al., 2000b; Wohl and Achyuthan, 2002; Richardson and Carling, 2005; Hsu et al., 2008).

Sharp-crested hummocky forms

The sharp crests of these features developed non-longitudinally and divided the convex form into two parts, having both a stoss side and a lee side (Fig. 7A1). The slope of the lee side (slope=0.65) was often steeper than that of the stoss side (slope=0.27). In the experiments, the sinuous crests were parallel to each other and the form of the convex parts was similar. The convex forms were arranged in rows with a regular spacing and orientation parallel to the flow direction (Fig. 7A1, A2), thereby producing regular trains of sharp-crested hummocky forms (Richardson and Carling, 2005).

Obstacle marks

Obstacle marks (Fig. 7B1 to B5) are the other typical composite erosional morphology found in the field (Baker, 1974; Lorenc et al., 1994; Richardson and Carling, 2005), and they were also commonly developed on all three experimental beds. In the field, obstacle marks are scour marks caused by flow separation and the horseshoe 'junction' vortex generated when flow encounters projections on the substrate (Simpson, 2001). These obstacle marks possess a crescentic planform shape (Allen, 1982), and in the present experiments they consisted of a raised projection as an obstacle with average width of 0.96 cm and a crescentic reversed furrow (average depth: 1.73 cm) upstream of it. The crescentic reversed furrows were parallel-sided in plan view with either open or closed ends.

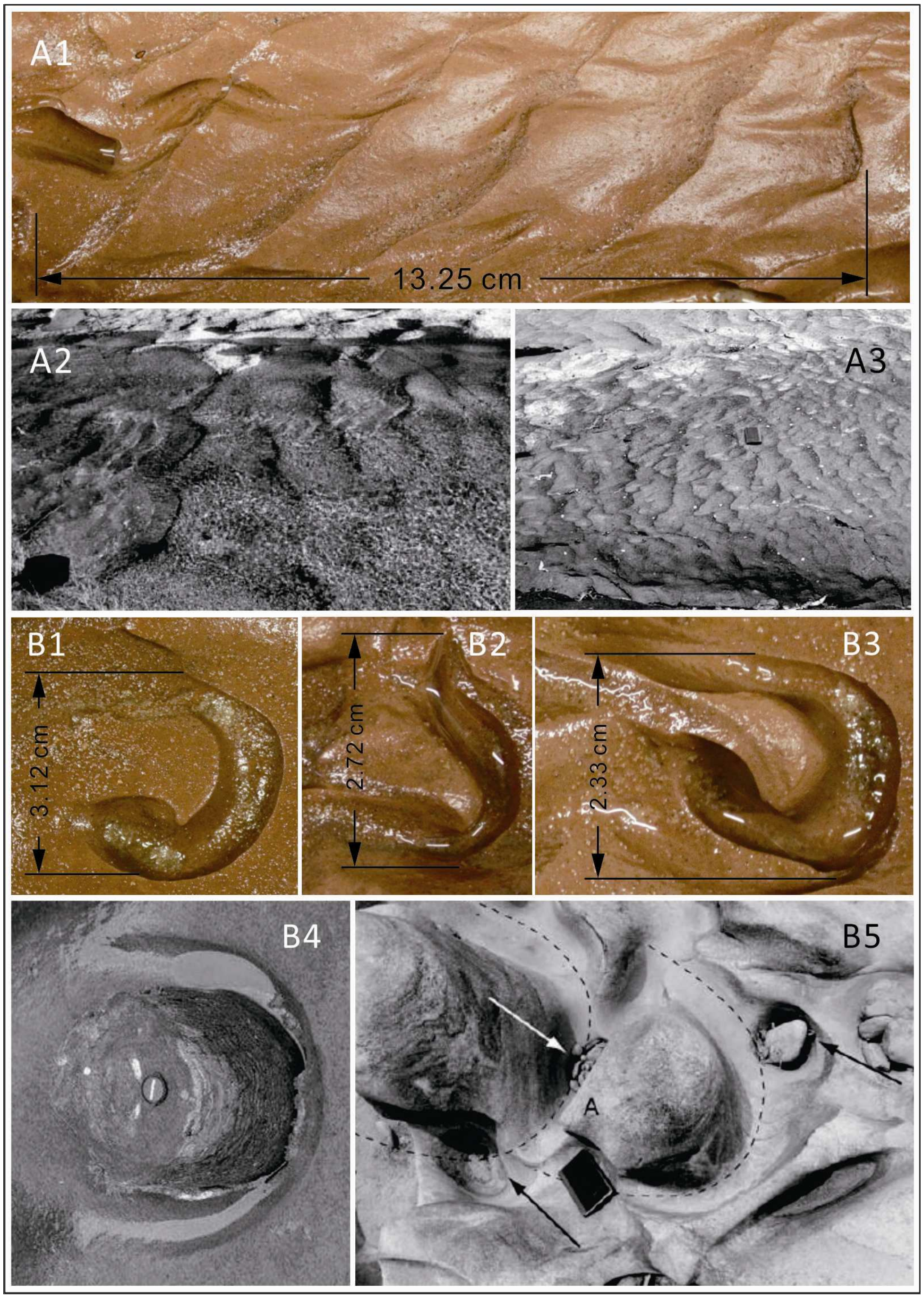

Figure 7. (1) Hummocky forms: A1: Regular trains of sharp-crested hummocky forms observed in Exp. 2. A2 and A3: hummocky forms found in natural bedrock surfaces, camera bag at the bottom left corner of A2, 0.20 m across, and a 0.15 m long handbook in A3, for scale (from Richardson and Carling (2005)). (2) Obstacle marks: B1, B2 are observed in Exp. 1 and B3 are in Exp. 2. B4 and B5: Obstacle marks observed in the field, the lens cap in B4 and the 0.15 m long handbook in B5 for scale (from Richardson and Carling (2005)).

Flow from right to left in all cases. A2, A3, B4 and B5 are reprinted from Richardson and Carling (2005) with permission from GSA.

4. Discussion

The three sediment-laden experiments described herein, using modelling clay with different initial shear strengths, produced a wide array of erosive bedforms that closely replicate many features observed in natural bedrock river substrates, including 7 kinds of potholes, 9 kinds of flutes, 15 kinds of furrows, and 4 examples of other bedforms (Appendix 1). The degree of similarity is so strong that many of the bedforms in the clay were almost identical to examples observed in the field (Figs 4-7). All of the forms were observed to originate on both flat beds and on a bed with initial defects, suggesting that initial bedrock defects are not critical for the genesis of bedforms, or for the overall variety of erosional forms. However, the imposed defects did have a significant effect on altering the specific type of bedform, especially in the genesis of obstacle marks (Fig. 7). The experiments indicated that although obstacle marks also developed on flat beds, they tended to form wherever small hollows were present irrespective of the size and depth of the defects. Whilst the present experiments reproduced the majority of the different bedforms recognised by Richardson and Carling (2005), there are a number of bedforms that were not observed in the current experiments (Appendix 1). Some of these features may be related to heterogeneities in natural substrates that were not present in the experiments. In addition, lateral features were not observed in the present experiments since all experiments utilised a flat bed. If the lack of substrate heterogeneity and lateral topography in the experiments is taken into account, then a remarkable range of forms observed in natural bedrock substrates were observed in the experiments.

Although all three experiments produced similar types of erosional forms, there were some differences in the diversity of forms between the different substrates, with experiment 2 (medium) showing the greatest diversity of forms. In the absence of repeat runs, the degree of variation between runs with nominally identical conditions cannot be quantified. Nonetheless, the present experiments suggest that for the given type of modelling clay, an undrained shear strength of 7.5 kPa, and a shear flow with initial basal shear stress of 4.8 Nm^{-2}, appears to provide the optimal characteristics for an analogue bedrock substrate for creating erosional bedforms.

In the present experiments, erosion is concentrated within the bedforms, widening and deepening them with time, whilst the areas between the bedforms have far less erosion.

The uniform cohesive substrate is unaffected by the plucking process, and similarly dissolution, corrosion and cavitation are not present given the conditions and timescales of the experiments. As a consequence, all erosion is caused by abrasion from the particulate load as confirmed by the initial clear water experiment. The concentration of erosion on the downstream side of bedforms (negative steps) suggests that the abrasion is closely coupled to the flow dynamics, rather than being caused by bed load saltation, in that the latter has been found to erode preferentially the upstream parts of bed protuberances (Whipple et al., 2000a). Calculation of the Rouse number, *Z*:

$$Z = \frac{W_S}{kU_*} \qquad \text{eq. 1}$$

where W_s is the sediment fall velocity, calculated here using the expression of (Gibbs et al., 1971), *K* is von Karman's constant taken as 0.4, and U_* is the shear velocity, provides an estimation of the transport condition of particles within a flow. For the experiments herein, Rouse numbers, *Z*, were ~0.4-0.6 for the D_{50} of 143 μm and ~1 for the D_{90} of 245 μm, and thus well below the suspension threshold of $Z<2.4$ (e.g., Lamb et al. (2015)), confirming that even the coarsest material was in suspension.

The present experiments are also the first to reproduce large surfaces composed of arrays of different and varied bedrock bedforms, and in marked contrast to previous experiments that tended to form a narrow range of features prior to formation of a single 'emergent channel' (Shepherd and Schumm, 1974; Wohl and Ikeda, 1997; Finnegan et al., 2007; Johnson and Whipple, 2007; Johnson and Whipple, 2010; Lamb et al., 2015). In part, this may reflect differences in initial conditions. Some previous experiments started with an initial channel (Shepherd and Schumm, 1974; Finnegan et al., 2007), or with the centre being lower than the edges (Johnson and Whipple, 2010), which will both encourage channelization. Other experiments possessed very shallow flow depths (0.02-0.03 m) that may have restricted macroturbulence and bedform development (Wohl and Ikeda, 1997). However, the experiments of Johnson and Whipple (2007) did start with initial planar bed conditions and greater flow depths (0.06-0.09 m), but still produced emergent channel geometries. A major difference between the present experiments and those of Johnson and Whipple (2007) is that the latter experiments were dominated by saltation-driven abrasion, rather than suspension-driven abrasion. This is reflected in Rouse numbers of 18-67 for the D_{50} of 2.5 mm, and 24-90 for the D_{90} of 3.76 mm based on Table 1 from Johnson and Whipple (2007) and calculating fall velocities with Gibbs et al. (1971). Other experiments have largely been undertaken with dominantly saltation-driven abrasion as reflected in their

Rouse numbers, Z ~2.3-6.2, with suspension-dominated abrasion only beginning to occur as narrower channels emerged (Wohl and Ikeda, 1997; Finnegan et al., 2007; Johnson and Whipple, 2007; Johnson and Whipple, 2010). A second important difference is that the present experiments were in the subcritical flow regime, Fr ~0.8, in contrast to previously published experiments that were all strongly supercritical, Fr ~1.4-3.5 (Wohl and Ikeda, 1997; Finnegan et al., 2007; Johnson and Whipple, 2007; Johnson and Whipple, 2010). These previous studies showed that the erosional morphologies are not sensitive to the magnitude of the Fr number, although the Fr numbers in those experiments were greater than that in natural bedrock rivers (Johnson and Whipple, 2007). Our experiments are consistant with those results and demonstrate that even when the flow is subcritical (Fr < 1), erosional bedforms can still be generated by flume-scale experiments with analogue bedrock substrates. Lastly, the present experiments do not exhibit brittle fracturing, unlike those experiments with concrete based or rock substrates or natural bedrock channels (Johnson and Whipple, 2007; Wilson et al., 2013; Lamb et al., 2015), suggesting that brittle fracturing is not important for the genesis of these bedrock features.

Field studies of polished rock surfaces sculpted by erosive bedforms have argued that these surfaces are dominated by suspension- rather than saltation-driven abrasion (Hancock et al., 1998; Whipple et al., 2000a). The present study provides support for these field studies, and provides experimental confirmation of the importance of suspension-driven abrasion in the genesis and maintenance of sculpted surfaces of erosive bedforms.

Some previous experiments have concentrated on the effects of bed load-driven saltation abrasion in order to answer a host of important questions, for example, the effects of varied bed load on the roughness of the bedrock substrate, incision rate and channel morphology (Hancock et al., 1998; Finnegan et al., 2007). Furthermore, the numerical saltation-load abrasion model (Sklar and Dietrich, 2004: Turowski et al., 2007) has been widely utilised to model bedrock river erosion from reach scales, through river profile development, to landscape evolution (e.g., Crosby et al., 2007; Cook et al., 2012; Egholm et al., 2013; Scheingross et al., 2014). However, there is increasing recognition that suspension-load abrasion is also important in many bedrock rivers, and that a total-load model incorporating the effects of abrasion from both saltation-load and suspension-load, is required for more accurate modelling of many of these processes (e.g., Lamb et al., 2008; Scheingross et al., 2014). Despite this recognition that suspension-load is important across a wide range of problems, there are a number of issues with extending existing experimental approaches to the suspension-dominated abrasion regime. Critically, the high tensile strengths of existing substrates coupled to the low angle of impact of suspension driven abrasion, means that large particles are required for any abrasion to occur (>0.2 mm for a range of natural bedrock, even in a ball mill; Sklar and Dietrich, 2001, 2004), and these particles require correspondingly high flow velocities to be transported in the suspension regime. Additionally, even for larger particles erosion rates across existing experimental substrates may be very low, restricting the utility of these substrates due to the large timescales required for measurable erosion. The present experiments demonstrate a method for extending the range of conditions that can be studied experimentally within realistic timescales, to this suspension-driven abrasion regime. The method presented herein thus opens up the potential to examine the temporal evolution of erosive bedrock features, the coupled effects of macroscopic turbulence and bedform development, and the interaction of multiple bedforms. In addition, this experimental approach enables study of the effects of incorporating suspension-load abrasion on landscape evolution, and to the development of total-load abrasion models incorporating suspension-load abrasion.

5. Conclusion

Our experiments produced bedforms highly analogous to natural field examples, and for the first time reproduced the overwhelming majority of bedform types that have been shown to occur on planar surfaces in homogenous substrates. The experiments reported herein confirm field observations that such surfaces and their erosive bedforms are primarily the result of suspension-driven abrasion, rather than bed load driven saltation dominated abrasion. It is also evident that cavitation, dissolution, corrosion, plucking, and supercritical flow conditions are not required for the generation of these forms. Whilst the clay substrates used here do not exhibit brittle fracturing due to discontinuities, experiments were able to reproduce a variety of erosive bedforms. This new method provides a viable approach for extending the physical modelling of saltation driven abrasion, to the suspension-dominated abrasion regime, within realistic laboratory timescales. This approach using modelling clay thus opens up the potential to study the evolution and fluid-bedform coupling of these bedforms, as well as experimentally examine the influence of suspension-dominated abrasion on landscape evolution.

Acknowledgements

This research was supported by Leeds-CSC Scholarship. We are particularly grateful to Gareth Keevil and Russell Dixon at the Sorby Laboratory, University of Leeds, for their extensive help designing and preparing the experimental setup. We would especially like to thank Wayne Stephenson for constructive comments on an early version of this manuscript.

References

Alexander, H.S., 1932. Pothole erosion. The Journal of Geology 40, 305-337.

Allen, J.R.L., 1969. Erosional current marks of weakly cohesive mud beds. Journal of Sedimentary Research 39(2), 607-623.

Allen, J.R.L., 1971. Transverse erosional marks of mud and rock: their physical basis and geological significance. Sedimentary Geology 5(3), 167-385.

Allen, J.R.L., 1982. Sedimentary structures: their character and physical basis, Volume 2. Elsevier Scientific, Amsterdam, pp. 663.

Ängeby, O., 1951. Pothole erosion in recent waterfalls. Lund Studies in Geography, Series A 2, 1-34.

Baker, V.R., 1973. Paleohydrology and sedimentology of the Lake Missoula flooding in eastern Washington. Geol. Soc. Am. Spec. Pap. 144, 1-73.

Baker, V.R., 1974. Erosional forms and processes for the catastrophic Pleistocene Missoula floods in eastern Washington. In: Morisawa, M. (Ed.,) Fluvial Geomorphology, Allen and Unwin, London, 123-148.

Baker, V.R., Kale, V.S., 1998. The role of extreme floods in shaping bedrock channels. In: Tinkler, K.J., Wohl, E.E. (Eds.), Rivers over Rock: Fluvial Processes in Bedrock Channels, American Geophysical Union Geophysical Monograph Series 107, 153-166.

Baker, V.R., Pickup, G., 1987. Flood geomorphology of the Katherine Gorge, Northern Territory, Australia. Geological Society of America Bulletin 98(6), 635-646.

Best, J.L., Kirkbride, A.D., Peakall, J., 2001. Mean flow and turbulence structure of sediment-laden gravity currents: new insights using ultrasonic Doppler velocity profiling. In: McCaffrey, W.D., Kneller, B.C., Peakall, J. (Eds.), Particulate Gravity Currents. International Association of Sedimentology Special Publication 31, Blackwell Science, Oxford, pp. 159–172.

Carling, P.A., Herget, J., Lanz, J.K., Richardson, K., Pacifici, A., 2009. Channel-scale erosional bedforms in bedrock and in loose granular material: Character, processes and implications. In: Burr, D.M., Carling, P.A., Baker, V.R. (Eds.), Megaflooding on Earth and Mars, pp. 13-32.

Carter, C.L., Anderson, R.S., 2006. Fluvial erosion of physically modeled abrasion dominated slot canyons. Geomorphology 81, 89–113.

Cook, K.L., Turowski, J.M., Hovius, N., 2012. A demonstration of the importance of bedload transport for fluvial bedrock erosion and knickpoint propagation. Earth Surface Processes and Landforms, 38, 683–695.

Crosby, B.T., Whipple, K.X., Gasparini, N.M., Wobus, C.W., 2007. Formation of fluvial hanging valleys: Theory and simulation. Journal of Geophysical Research, 112, F3, doi:10.1029/2006jf000566.

Dzulynski, S., 1965. New data on experimental production of sedimentary structures. Journal of Sedimentary Petrology 35, 196-212.

Dzulynski, S., 1996. Erosional and deformational structures in single sedimentary beds: a genetic commentary. Annals Societatis Geologorum Poloniae 66, 101-189.

Dzulynski, S., Sanders, J.E., 1962. Current marks on firm mud bottoms. Trans. of the Connecticut Academy of Arts and Sciences 42, 57-96.

Dzulynski, S., Walton, E.K., 1963. Experimental production of sole marking. Trans. of the Edinburgh Geological Society, 19 279-305.

Egholm, D., Knudsen, M., Sandiford, M., 2013. Lifespan of mountain ranges scaled by feedbacks between landsliding and erosion by rivers. Nature, 498, 475–478.

Elston, E.D., 1917. Potholes: their variety, origin and significance. The Scientific Monthly 5, 554-567.

Elston, E.D., 1918. Potholes: their variety, origin and significance. II. The Scientific Monthly 6, 37-51.

Engel, P., 1976. Impact Wear of Materials. Elsevier Science Ltd, New York, pp 356.

Finnegan, N.J., Sklar, L.S., Fuller, T.K., 2007. Interplay of sediment supply, river incision, and channel morphology revealed by the transient evolution of an experimental bedrock channel. J. Geophys. Res. Earth Surf. 112 (F3), F03S11.

Gibbs, R.J., Matthews, M.D., Link, D.A., 1971. The relationship between sphere size and settling velocity. Journal of Sedimentary Petrology 41, 7-18.

Hancock, G.S., Anderson, R.S., Whipple, K.X., 1998. Beyond power: Bedrock river incision process and form. In: Tinkler, K.J., Wohl, E.E. (Eds.), Rivers over Rock: Fluvial Processes in Bedrock Channels, American Geophysical Union Geophysical Monograph Series 107, 35-60.

Hsu, L., Dietrich, W.E., Sklar, L.S., 2008. Experimental study of bedrock erosion by granular flows. J. Geophys. Res.-Earth Surf. 113, F02001.

Ives, R.L., 1948. Plunge pools, potholes, and related features. Rocks and Minerals 23(1), 3-10.

Jennings, J.N., 1983. Swirlholes and related bedrock river channel forms. The Australian Geographer, 15(6) 411-414.

Johnson, J.P., Whipple, K.X., 2007. Feedbacks between erosion and sediment transport in experimental bedrock channels. Earth Surf. Process. Landf. 32, 1048-1062.

Johnson, J.P., Whipple, K.X., 2010. Evaluating the controls of shear stress, sediment supply, alluvial cover, and channel morphology on experimental bedrock incision rate. Journal of Geophysical Research: Earth Surface 115(F2), F02018.

King, P.B., 1927. Corrosion and Corrasion on Barton Creek, Austin, Texas. The Journal of Geology 35, 631-638.

Kor, P.S.G., Cowell, D.W., 1998. Evidence for catastrophic subglacial meltwater sheetflood events on the Bruce Peninsula, Ontario. Canadian Journal of Earth Sciences 35(10), 1180-1202.

Lamb, M.P., Dietrich, W.E., Sklar, L.S., 2008. A model for fluvial bedrock incision by impacting suspended and bed load sediment. Journal of Geophysical Research, 113, doi:10.1029/2007JF000915.

Lamb, M.P., Finnegan, N.J., Scheingross, J.S., Sklar, L.S., 2015. New insights into the mechanics of fluvial bedrock erosion through flume experiments and theory. Geomorphology, doi: 10.1016/j.geomorph.2015.03.003.

Lamb, M.P., Fonstad, M.A., 2010. Rapid formation of a modern bedrock canyon by a single flood event. Nat. Geosci. 3 (7), 477–481.

Lorenc, M.W., Barco, P.M., Saavedra, J., 1994. The evolution of potholes in granite bedrock, W Spain. Catena 22(4), 265-274.

Maxson, J.H., Campbell, I., 1935. Stream fluting and stream erosion. The Journal of Geology 43, 729-744.

Peakall, J., Ashworth, P., Best, J., 1996. Physical Modelling in Fluvial Geomorphology: Principles, Applications and Unresolved Issues. In: Rhoads, B.L., Thorn, C.E. (Eds.), The Scientific Nature of Geomorphology. John Wiley and Sons, Chichester, 221-253.

Richardson, K., Carling, P.A., 2005. A Typology of Sculpted Forms in Open Bedrock Channels. Geological Society of America Special Paper 392, pp. 108.

Scheingross et al., J.S., Brun, F., Lo, D.Y., Omerdin, K., Lamb, M.P., 2014. Experimental evidence for fluvial bedrock incision by suspended and bedload sediment. Geology, 42, 523-526.

Shepherd, R.G., Schumm, S.A., 1974. Experimental study of river incision. Geol. Soc. Am. Bull. 85, 257–268.

Simpson, R.L. 2001. Junction Flows, Annu. Rev. Fluid Mech., 33, 415–43.

Sklar, L.S., Dietrich, W.E., 2001. Sediment and rock strength controls on river incision into bedrock. Geology 29(12), 1087-1090.

Sklar, L.S., Dietrich, W.E., 2004. A mechanistic model for river incision into bedrock by saltating bed load. Water Resour. Res. 40(6), W06301.

Tinkler, K.J., 1993. Fluvially sculpted rock bedforms in Twenty Mile Creek, Niagara Peninsula, Ontario. Canadian Journal of Earth Sciences 30(5), 945-953.

Tinkler, K.J., 1997. Rockbed wear at a flow convergence zone in Fifteen Mile Creek, Niagara Peninsula, Ontario. The Journal of Geology 105(2), 263-274.

Turowski, J.M., Lague, D., Hovius, N., 2007. Cover effect in bedrock abrasion: A new derivation and its implications for the modeling of bedrock channel morphology. Journal of Geophysical Research, 112, doi:10.1029/2006JF000697.

Whipple, K.X., Hancock, G.S., Anderson, R.S., 2000a. River incision into bedrock: Mechanics and relative efficacy of plucking, abrasion, and cavitation. Geological Society of America Bulletin 112(3), 490-503.

Whipple, K.X., Snyder, N.P., Dollenmayer, K., 2000b. Rates and processes of bedrock incision by the Upper Ukak River since the 1912 Novarupta ash flow in the Valley of Ten Thousand Smokes, Alaska. Geology 28(9), 835-838.

Wilson, A., Lavé, J., 2014. Convergent evolution of abrading flow obstacles: Insights from analogue modelling of fluvial bedrock abrasion by coarse bedload. Geomorphology 208, 207-224.

Wilson, A., Hovius, N., Turowski, J.M., 2013. Upstream-facing convex surfaces: Bedrock bedforms produced by fluvial bedload abrasion. Geomorphology 180-181, 187-204.

Wohl, E.E., 1992. Bedrock benches and boulder bars: Floods in the Burdekin Gorge of Australia. Geological Society of America Bulletin 104(6), 770-778.

Wohl, E.E., 1993. Bedrock channel incision along Piccaninny Creek, Australia. The Journal of Geology 749-761.
Wohl, E.E., 1998. Bedrock channel morphology in relation to erosional processes. In: Tinkler, K.J., Wohl, E.E. (Eds.), Rivers over Rock: Fluvial Processes in Bedrock Channels, American Geophysical Union Geophysical Monograph Series 107, 133-152.
Wohl, E.E., Achyuthan, H., 2002. Substrate influences on incised-channel morphology. The Journal of Geology 110(1), 115-120.
Wohl, E., Ikeda, H., 1997. Experimental simulation of channel incision into a cohesive substrate at varying gradients. Geology 25, 295–298.
Wohl, E.E., Ikeda, H., 1998. Patterns of bedrock channel erosion on the Boso Peninsula, Japan. J. Geol. 106(3), 331-345.
Yin, D., 2013. Genesis and Evolution of Bedforms on Cohesive Mud Beds and Simulated Bedrock Channels. PhD thesis, University of Leeds, UK, pp. 309.
Zen, E., Prestegaard, K.L., 1994. Possible hydraulic significance of two kinds of potholes: Examples from the paleo-Potomac River. Geology 22(1), 47-50.

Appendix

Appendix 1**.** Bedform types and dimensions observed in the present experiments, and comparison with those described by (Richardson and Carling, 2005)**. Remarks indicate which experiment features observed from.**

	Types of bedforms	Rock type	Length (cm)	Width (cm) (lower parts)	Depth (cm)	Remarks
Pothole	Ovoid pothole	Fine-grained sandstone	0.85 1.27	1.20 1.35	1.08 1.61	Fig. 4: A1-Exp. 2 : A2-Exp. 2
	Spiral-furrowed pothole	Microgranite	4.96 2.69	2.92 3.52	2.21 2.45	Exp. 1 Exp. 2
	Incipient pothole	Limestone	-	-	-	-
	Pothole with entry furrow	Calcareous mudstone	2.67 3.96	1.29 1.31	0.96 2.20	Fig. 4: D1-Exp. 2 : D2-Exp. 2
	Pothole with extended exit furrow	Granitic gneiss	3.69 3.31	0.81 1.06	1.60 1.60	Fig. 4: B1-Exp. 2 : B3-Exp. 2

	Open pothole	Fine- grained sandstone	2.41	1.54	2.71	Fig. 4: C1-Exp. 2
	A pothole with horizontal furrows	Calcareous mudstone	-	-	-	-
	Hierarchical pothole	Granitic gneiss	5.03 3.82	4.38 3.03	2.55 2.33	Exp. 1 Exp. 3
	Convoluted pothole	Gneiss	9.46 1.73	5.92 1.25	2.76 1.04	Exp. 1 Exp. 3
	Large isolated breached pothole	Granitic gneiss	-	-	-	-
	Coalesced potholes	Granitic gneiss	-	-	-	-
	Natural arch	Granitic gneiss	-	-	-	-
	Natural pillar	Granitic gneiss	-	-	-	-
	Closed lateral pothole	Granitic gneiss	-	-	-	-
	Lateral pothole	Granitic gneiss	-	-	-	-
	Conjugate linear lateral potholes	Granitic gneiss	-	-	-	-
	Compound lateral pothole of the hierarchical variety	Granitic gneiss	-	-	-	-
	Paired lateral potholes	Dolomit	-	-	-	-
Flute	Broad flute	Limestone	0.94	2.75	0.59	Exp. 2
	Narrow flute	Granitic gneiss	1.56	0.79	0.56	Exp. 2
	Flute with median ridge and internal secondary structures	Calcareous mudstone	2.65	1.47	1.07	Exp. 2
	Spindle-shaped flute	Rhyolitic agglomerate	2.62	0.65	0.59	Exp. 2

	Flute with internal secondary structures	Calcareous mudstone	2.41 3.09 2.71	1.44 2.49 1.34	1.43 0.69 0.47	Fig. 5: A1-Exp. 1 : B1-Exp. 2 : B2-Exp. 2
	Flute with external secondary structures	Limestone	6.38 3.99 7.88 3.01	1.41 1.33 2.44 1.14	0.65 0.84 0.71 1.25	Fig. 5: C1-Exp. 2 : C2-Exp. 2 : C3-Exp. 2 : C4-Exp. 3
	En echelon flutes	Granitic gneiss	4.75	4.15	1.28	Exp. 2
	Paired flutes	Granitic gneiss	2.89	2.07	1.24	Exp. 1
	Lineations	Limestone	8.06	9.01	0.10	Exp. 2
Furrow	Straight short furrow	Limestone	2.09 2.52	0.82 0.80	1.50 0.99	Fig. 6: A1-Exp. 1 : A3-Exp. 2
	Curved short furrow	Calcareous mudstone	2.87	0.63	1.55	Exp. 2
	Cuspate, deep short furrow	Gneiss	2.09 2.52	0.82 0.80	1.50 0.99	Fig. 6: A1-Exp. 1 : A3-Exp. 2
	Paired short furrows	Calcareous mudstone	-	-	-	-
	Short furrow with internal secondary structures	Gneiss	-	-	-	-
	Straight parallel-sided furrow	Fine-grained sandstone	2.81	0.51	1.24	Exp. 2
	Curved parallel-sided furrow	Granitic gneiss	3.91	0.35	1.22	Exp. 2
	Sinuous parallel-sided furrow	Fine-grained sandstone	1.29 3.61 16.22	0.54 0.31 0.90	1.19 1.22 1.90	Fig. 6: B1-Exp. 3 : B3-Exp. 2 : B4-Exp. 1
	Parallel-sided furrow with levees	Fine-grained sandstone	-	-	-	-
	Chute furrow	Limestone	-	-	-	-

Chimney furrow	Interbedded limestone and marl	-	-	-	-
Bifurcating furrows	Microgranite	4.71 23.11	2.68 1.45 (bifurcating point)	1.50 1.50	Exp. 2 Exp. 3
Group of parallel-sided furrows	Limestone	2.20 (average)	0.68 (average)	0.76 (average)	Exp. 2
Regular compound parallel-sided furrows	Andesite	10.24	0.98	1.90	Exp. 2
Irregular compound parallel-sided furrows	Limestone	10.62 10.52	0.37 0.61	1.22 1.34	Exp. 2
Funnel-shaped furrow (underwater)	Medium-grained sandstone	2.44	1.62	0.56	Exp. 2
Bulbous furrow (underwater)	Fine-grained sandstone	3.28	1.55	1.10	Exp. 2
Runnel with cusped margins	Fine-grained sandstone	-	-	-	-
Oblique sloping furrows	Granitic gneiss	-	-	-	-
Compound transverse furrows	Fine-grained sandstone	-	-	-	-
Cross-channel furrow (underwater).	Fine-grained sandstone	-	-	-	-
Straight reversed furrow	Granitic gneiss	-	-	-	-
Curved reversed furrow	Granitic gneiss	4.02	0.61	2.00	Exp. 3
Open-ended reversed furrow	Granitic gneiss	5.79	4.07	2.08	Exp. 1
Branched reversed furrow	Granitic gneiss	-	-	-	-

	Group of parallel reversed furrows	Granitic gneiss	3.28	2.78	1.68	Exp. 1
Convex and undulating surfaces	Convergent furrow complex	Granitic gneiss	6.66	1.96	1.08	Exp. 2
	Yin- yang furrow complex	Calcareous mudstone	-	-	-	-
	Nested curved furrow complex	Medium-grained sandstone	-	-	-	-
	Overhanging concave surface	Granitic gneiss	-	-	-	-
	Cavetto	Limestone	-	-	-	-
	Taffoni	Fine-grained sandstone	-	-	-	-
	Shallow concave surfaces	Calcareous mudstone	-	-	-	-
	Hummocky forms	Limestone	13.25	3.50	0.59	Fig. 7: A1-Exp. 2
	Pseudoripples	Andesite	-	-	-	-
	Microripples	Gneiss	-	-	-	-
	Partially abraded surface	Limestone	-	-	-	-
	Bladed forms	Calcareous mudstone	3.31 7.40	1.93 0.97	0.74 1.60	Exp. 2
	Obstacle mark (Current crescents with secondary sculpting)	Rhyolitic agglomerate	3.12 2.72 2.33	2.38 (0.79) 1.746 (0.47) 2.99 (0.76)	1.84 1.69 1.66	Fig. 7: B1-Exp. 1 : B2-Exp. 1 : B3-Exp. 2
	Pseudoripples with short furrows	Andesite	-	-	-	-
	Runnel with SCHF	Gneiss	-	-	-	-
	Parallel runnels with step-pool structures	Granite	-	-	-	-

High relief Hummocky forms with current crescents	Limestone	-	-	-	-
Hummocky forms with steep lee faces	Limestone	-	-	-	-

Bedform genesis in bedrock substrates: insights into formative processes from a new experimental approach and the importance of suspension-dominated abrasion

Daowei Yin[1,2]*

[1] School of Earth and Environment, University of Leeds, Leeds, UK;

[2] State Key Laboratory of Coastal and Estuarine Research, East China Normal University, Shanghai 200062, China. Nicholas_t_yin@hotmail.com;

* Corresponding author

Jeff Peakall[1]

[1] School of Earth and Environment, University of Leeds, Leeds, UK. J.Peakall@leeds.ac.uk;

Dan Parsons[3]

[3] Department of Geography, Environment and Earth Science, University of Hull, Hull, UK. d.parsons@hull.ac.uk;

Zhongyuan Chen[2]

[2] State Key Laboratory of Coastal and Estuarine Research, East China Normal University, Shanghai 200062, China. z.chen@ecnu.edu.cn;

Heather Macdonald[1,4]

[1] School of Earth and Environment, University of Leeds, Leeds, UK;

[4] ExxonMobil Exploration Company, 222 Benmar Drive, Houston, Texas 77060, USA. h.macdonald@see.leeds.ac.uk;

Paul Wignall[1]

[1] School of Earth and Environment, University of Leeds, Leeds, UK. P.B.Wignall@leeds.ac.uk;

Jim Best[5]

[5] Departments of Geology, Geography and GIS, Mechanical Science and Engineering and Ven Te Chow Hydrosystems Laboratory, University of Illinois, Urbana-Champaign, IL 61801, USA. jimbest@illinois.edu.

Abstract

Bedrock channels are common in the natural environment and bedrock channel erosion sets the pace of denudation in many of the world's river catchments. However, there have been very few investigations that concern either bedrock bedform genesis or bedrock channel abrasion processes. Field based analysis of sculptured forms within bedrock channels has been restricted notably by the slow rate of bedform development in such environments. Few flume-scale experiments have been conducted that attempt to simulate the genesis of sculpted bedforms in bedrock channels. This study demonstrates that optimisation of clay beds through successfully matching clay strength enables the development of features analogous to bedrock river channel bedforms. Three sets of sediment-laden experiments were carried out using hard, medium and soft clay beds, respectively. A suite of erosive bedforms, including potholes, flutes, and furrows developed on all experimental beds. All observed erosional features have clear equivalents to those observed in natural bedrock rivers. This work further demonstrates that in the absence of suspended sediment, fluid flow cannot induce erosion in cohesive or bedrock substrates. Basal shear strength was a significant factor for the genesis of different types of simulated bedrock bedforms in our experiments. Lastly this work illustrates that abrasion by suspended sediments is the only driving force necessary for the formation of these bedrock bedforms, because the erosional features were produced in the absence of bed load abrasion, plucking, cavitation and dissolution.

1. Introduction

Bedrock rivers exhibit a diverse array of erosional forms, that in turn influence flow fields and sediment dynamics (Richardson and Carling, 2005). The genesis and formative processes of these erosional features is poorly understood, and remains an area where there is a major knowledge gap (Lamb et al., 2015). This is largely because field studies are limited by the slow rate of development of erosion within bedrock substrates, and by the difficulty and danger of attempting to measure processes during infrequent high magnitude flow events (Lamb et al., 2015). Physical experiments offer the opportunity to examine processes at much faster development rates, and under controlled conditions (Peakall et al., 1996; Lamb et al., 2015). However, there have been relatively few studies of erosive bedforms in substrates analogous to those observed in bedrock rivers (Shepherd and Schumm, 1974; Wohl and Ikeda, 1997; Carter and Anderson, 2006; Johnson and Whipple, 2007; Johnson and

Whipple, 2010; Wilson et al., 2013; Wilson and Lave, 2014). Furthermore, these studies have only reproduced a small number of the features identified in natural channels (Richardson and Carling, 2005). Model studies on actual rock substrates have been restricted to forming upstream facing convex surfaces (Wilson et al., 2013; Wilson and Lave, 2014). In contrast, studies utilising artificial substrates exhibit a wider range of features, with those on concrete (Carter and Anderson, 2006; Johnson and Whipple, 2007; Johnson and Whipple, 2010) and mixed sand/mud substrates (Shepherd and Schumm, 1974; Wohl and Ikeda, 1997) producing longitudinal grooves, potholes, and furrows. Even in these cases, experiments with initially broad erosion surfaces are dominated by longitudinal grooves that over time form 'emergent channel geometries' (Shepherd and Schumm, 1974; Wohl and Ikeda, 1997; Finnegan et al., 2007; Johnson and Whipple, 2007; Johnson and Whipple, 2010; Lamb et al., 2015). Consequently, despite these advances, experiments have failed to produce the wide variety of bedforms observed in natural systems, and the broad spatial distribution of these erosive features. In turn, this raises questions as to the nature of the experimental conditions and physical processes required to reproduce many of these bedrock bedforms. Here, we utilise compacted clay substrates to reproduce most of the observed features present in bedrock rivers (c.f. Richardson and Carling (2005)). The nature of the formative conditions are discussed and compared to existing physical modelling and field studies.

1.1. Previous erosional experiments with clay beds

Although clay substrates have been used to study erosional bedforms in physical experiments, these studies produced features such as flutes and longitudinal grooves that have been compared to natural erosion in cohesive muddy substrates such as deep-sea muds and river floodplains (e.g., Dzulynski and Sanders, 1962; Dzulynski and Walton, 1963; Dzulynski, 1965, 1996; Allen, 1969,1971). Furthermore, the applicability of these mud-rich cohesive sediments to bedrock rivers has been questioned (e.g., Lamb et al. (2015)) because of the absence of brittle fracturing that typically occurs in bedrock erosion (Engel, 1976). The majority of experiments that have been undertaken on weak muddy substrates, typically used beds formed from *in situ* settling of clays in water for periods of hours to days (e.g., Dzulynski and Walton, 1963; Dzulynski, 1965, 1996; Allen, 1969, 1971), producing a range of features such as flutes and groove marks. In contrast, there has been very little work on firm or hard mud beds. Allen (1971) undertook a series of 13 experiments in a Perspex pipe, where particulate-flows eroded beds of kaolin-based modelling clay, producing flute like features. Run times were between 27 and 74 minutes, although these experiments could not be continued beyond these timescales as a series of bed waves developed (Allen, 1971).

Dzulynski and Sanders (1962) also used modelling clay to examine tool marks, but these experiments were undertaken by rolling objects by hand across subaerially exposed clay. Whilst these experiments on weak and firm clay beds have demonstrated a range of erosive features, there is an absence of quantitative data on substrate strength, such as the shear strength, and on flow properties such as basal shear stress, with which to explore the boundary conditions of such erosive features. The experiments presented here revisit the utility of clay substrates for modelling bedrock erosion, but under conditions where the substrate strength and basal shear stress are quantified, and we examine the development of erosive features in the absence of brittle fracturing.

1.2. Erosive mechanisms in bedrock substrates

The major erosional mechanisms postulated to control the morphology and genesis of bedrock channels are: (1) abrasion (Hancock et al., 1998; Wohl, 1998; Whipple et al., 2000a; Sklar and Dietrich, 2001; Sklar and Dietrich, 2004; Johnson and Whipple, 2007; Wilson et al., 2013; Wilson and Lave, 2014); (2) plucking (Baker, 1973; Hancock et al., 1998; Whipple et al., 2000a; Whipple et al., 2000b; Lamb and Fonstad, 2010); (3) cavitation (Baker, 1974; Wohl, 1992; Baker and Kale, 1998; Hancock et al., 1998; Wohl, 1998; Whipple et al., 2000a; Whipple et al., 2000b); and (4) dissolution or corrosion (Wohl, 1992; Wohl, 1998; Whipple et al., 2000a). Of these, abrasion and plucking are considered the most important processes, with plucking effective when rocks are fractured and exhibit discontinuities, whilst abrasion is thought to dominate in massive rock with weak jointing (Hancock et al., 1998; Whipple et al., 2000a; Lamb and Fonstad, 2010). Abrasion can occur as a result of either saltating bed load or as suspended-load, with debate on the relative efficacy of these two modes in bedrock rivers (Hancock et al., 1998; Whipple et al., 2000a). Evidence for the importance of cavitation in the field and experiments is lacking, although theoretically it is thought to be a plausible contributing factor (Whipple et al., 2000a; Carling et al., 2009). Weathering of bedrock through corrosion may also be important, but has been little studied using experiments (Lamb and Fonstad, 2010).

2. Methodology

A series of four experimental runs were undertaken to examine the nature of erosion in clay beds by open channel flow, three containing a particulate load of fine-grained sand and one without particulate load (clear water). Air-dried modelling clay was used as the substrate, with the initial undrained shear strength of the clay beds adjusted between runs through pre-soaking of the clay bed.

Experimental setup

An 8.75 m long, tilting, recirculating hydraulic slurry flume (0.30 m wide by 0.30 m deep) was used for the experiments (Fig. 1). The flume contained a false floor into which a tray (0.90 m long and 0.075 m deep) containing clay could be inserted, such that the upper surface of the clay-bed was flush with the false floor (Fig. 1). The water depth was set to 0.14 m above the clay bed in all experiments, and uniform flow was obtained by adjusting the flume slope to 0.005. An array of ten 4 MHz ultrasonic Doppler velocimetry probes (UDVP; (Best et al., 2001)) were positioned downstream of the clay bed, pointing upstream, with the ends of the transducers positioned level with the end of the clay bed (Fig. 1). The UDVP collected data for 99 seconds at a temporal resolution of 8 Hz; the operating parameters for the UDVP are shown in Table 1. The UDVP probes enabled flow velocity profiles, initial basal shear stress (Exp. 1: $\tau \approx 3.10$ Nm^{-2}; Exp. 2: $\tau \approx 4.85$ Nm^{-2}; no data for Exp. 3 but of similar order to experiments 1 and 2), and mean flow velocity (V_{mean} = 0.75-0.81 ms^{-1}), to be measured above the clay bed. A further experiment (Exp. 4) was run for 12 hours without a sediment load or bed defects, with an undrained shear strength of 10.5 kPa, initial basal shear stress of 3.10 Nm^{-2} and flow velocity of ~0.81 ms^{-1}. Water temperature during the experiments varied between 8-10°C.

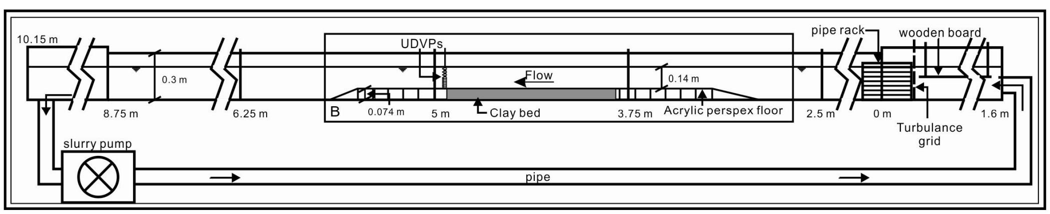

Figure 1. Schematic drawing of the experimental setup of the hydraulic slurry flume. The dark area represents the clay bed with a tray that was lowered into position so that the top surface of the clay bed was flush with the surrounding false floor.

Table 1. Parameters for the UDVP used in the presented experiments

Ultrasonic frequency	Bin Width	Bin distance	Measurement window	Number of bins	Multiplexing time delay	Number of profiles per transducer	Ultrasound velocity	Transducer diameter	Bins for analysis
4 MHz	1.48 mm	0.74 mm	5-101.2 mm	128	15 ms	500	1480 ms^{-1}	8 mm	31-38

Clay preparation and undrained shear strength measurement

Air-dried modelling clay (Potter's Scola Clay) was used as the substrate and consisted primarily of illite-smectite, kaolinite and quartz (Table 2). The pre-soaking time was altered to adjust the initial undrained shear strength of the substrate from 10.5 kPa (Exp. 1), through 7.5 kPa (Exp. 2) to 5.5 kPa (Exp. 3) (Fig. 2) - referred to herein as hard, medium and soft. Shear strength was measured using a hand shear vane meter with a four-blade vane (25.4 mm wide by 50.8 mm deep). After soaking to the required strength, the clay was placed in a tray and inserted into the flume. In order to ensure the original bed surface was flat the clay surface was smoothed by hand using a metal board to the same level as the surrounding Perspex floor.

Table 2 X-ray diffraction analysis of modelling clay used in the experiments

	Quartz	Illite-smectite	Kaolinite	Hematite
Chemical composition (%)	35.3	39.1	21.1	4.5

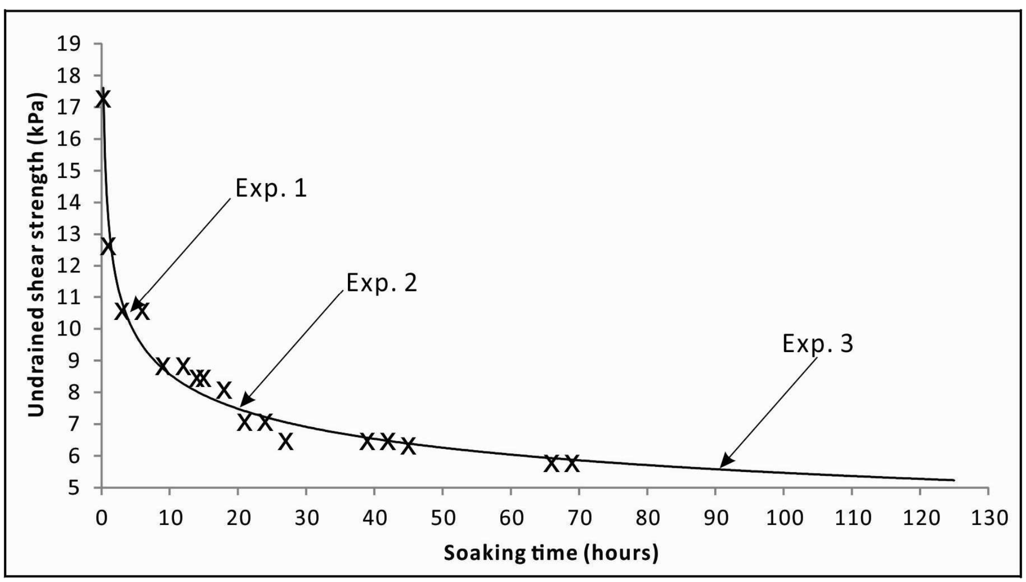

Figure 2 Variation in undrained shear strength with soaking time. Positions of the initial undrained shear strengths are shown for each experiment; Exp. 1: Hard: 10.5 kPa; Exp. 2: Medium: 7.5 kPa; Exp. 3: Soft: 5.5 kPa.

Experimental conditions

Experiments were initiated with both smooth clay beds (Exps. 2 and 3) and with a number of circular bed defects (Exp. 1; Fig. 3). The defects consisted of five large holes 2.4

cm in diameter and 0.3 cm in depth, two medium-sized hollows 0.9 cm in diameter and 0.2 cm in depth, and 2 smaller holes 0.6 cm in diameter and 0.2 cm in depth (Exp. 1; Fig. 3). Each experiment was then run until no further morphological change of the clay bed was observed, in part corresponding with the substrate beginning to be covered by sand deposited from suspension. Consequently the total run times of experiments 1-3 (hard, medium, soft) were 1680 min, 1800 min, and 1080 min respectively. The experiments were stopped periodically in order to take photographs after slowly draining the flume (e.g., Fig. 3b). These breaks in each experimental run took place at 1 and 2 hours and then every 2 hours until the end of the experiment, with an additional sampling point at 30 minutes for experiment 1. In order to rectify the distorted photographs, four straight control bars with 10 control points on each of them were distributed around the edges of the clay bed and corrections were undertaken using DxO ViewPoint software. Silica sand with a D_{10} of 82 µm, D_{50} of 143 µm, and D_{90} of 245 µm was added to the flow. In order to maintain a constant suspended sediment concentration (SSC), 1.5 kg of sand was progressively introduced every 15 minutes, thus compensating for sediment deposited in the pipework of the hydraulic flume. Sediment concentration was monitored via water samples collected at a depth of ~7 cm above the Perspex floor and ~10 cm downstream of the clay beds every 20 minutes; 95% of all SSC measurements were in the range of 0.10% to 0.20% by weight.

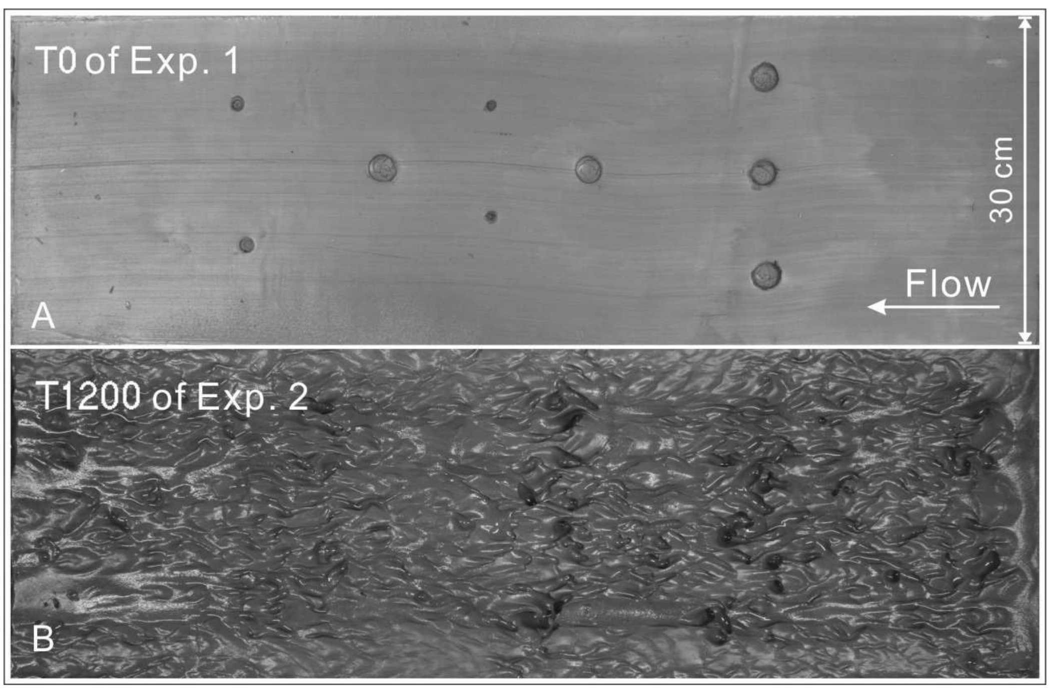

Figure 3 A: The initial experimental bed of Exp. 1: Hard, the pre-formed larger holes are 2.4 cm in diameter and 0.3 cm in depth; the medium-sized hollows are 0.9 cm in diameter and 0.2 cm in depth, and the smallest hollows are 0.6 cm in diameter and 0.2 cm in depth. B: The fully developed experimental bed of Exp. 2 after 1200 minutes run time. The initial bed of Exp. 2 was a flat bed without hollows. Flow was from right to left in both cases.

3. Results

Clear water experiment

The experiment undertaken without a sediment load or bed defects (Exp. 4) and run over 12 hours exhibited no bed erosion.

Evolution of the clay bed

The evolution and erosion rate of the clay bed differed between the three experiments with a suspended-load (Exps. 1-3) as a function of the undrained shear stress. For the hard clay bed (10.5 kPa), the bed barely altered until after 960 minutes and stopped eroding after 1440 minutes, whilst for the medium bed (7.5 kPa) bedforms initiated after 720 minutes and stopped eroding after 1320 minutes. The erosion of the softest experimental bed (5.5 kPa) began after 480 minutes and ended at 960 minutes, although this run was initiated with a series of bed defects restricting direct temporal comparison. Whilst bedform development occurred at different rates in experiments 1-3, the final forms in each showed strong similarities, with the three experiments producing an array of erosional features. Details of the most common types and geometries of these erosional features, including 4 types of potholes, 3 types of flutes, 2 types of furrows and 2 types of convex and undulating bedforms, are given below together with a comparison with natural bedrock sculpted forms.

3.1 Individual simulated erosional bedrock bedforms

Potholes

Potholes are the most common abrasion sculpture in bedrock channels (Elston, 1917; Elston, 1918; Alexander, 1932; Maxson and Campbell, 1935; Ives, 1948; Allen, 1971; Allen, 1982; Wohl, 1992; Wohl, 1993; Zen and Prestegaard, 1994; Wohl and Ikeda, 1998; Richardson and Carling, 2005) as well as the most commonly observed erosional features on the experimental clay beds. The potholes observed in the present experiments can be classified into the following categories of Richardson and Carling (2005): i) simple potholes; ii) potholes with extended exit furrows s; iii) open potholes; iv) spiral-furrowed potholes with a spiral rib ; v) spiral furrowed pothole; vi) potholes with both entry and extended exit furrows; vii) potholes with exit furrows; viii) potholes with horizontal furrows; ix) potholes with lateral external secondary furrows; x) complex potholes / convoluted potholes; and, xi) hierarchical potholes. Importantly potholes representing all 11 categories were observed. For brevity, only the details of the four most common types of pothole are described herein (Fig. 4). Extensive discussion of all the features observed is provided by Yin (2013).

Simple potholes

This kind of isolated, quasi-round pothole with a cylindrical form is common in natural bedrock channels, and was common in the current experiments (Fig. 4A1, A2. Note that dimensions of features are provided in the figures). Simple potholes could be observed on the bed as part of more complex features, or sometimes in the early stage of the experiments. These potholes typically evolved into other forms (e.g. flutes and short furrows), widening and deepening their quasi-round opening, and thus were rarely stable. The radius of the opening was usually slightly larger than that of the internal radius of its base, but the form is still regarded as approximately cylindrical. The diameter of the opening enlarged with time and extended in a specific direction, usually downstream, to form exit furrows. As a consequence, the rims of solitary potholes typically did not maintain a quasi-round geometry.

Potholes with extended exit furrows

Potholes with extended exit furrows were the most common pothole developed in the experimental beds (Fig. 4B1 to B4) The downstream ends of the exit furrows were not always closed and the lengths of the exit furrows were much bigger than the diameters of the primary potholes. The ratio of length to diameter ranges from 3.12 to 4.55 in the current case. The exit furrows usually exhibited a curved planform profile in the downstream direction with lengths more than twice as long as the widths. These features were still considered potholes because they developed from individual hollows located at the upstream end that are much deeper than the rest of the bedforms. The rims of these exit furrows were parallel, and in some cases they were closed at their downstream end (Fig. 4B1, B2). In other cases, the exit furrows were totally open at their downstream ends (Fig. 4B3, B4). Individual simple potholes could develop in time into potholes with extended exit furrows, or open potholes, if they did not connect to adjacent bedforms.

Open potholes

Open potholes are a kind of pothole that has an open end in plan view (Fig. 4C1, C2) that is almost as wide as the diameter of the primary hollow. These open potholes usually lack a lee side edge and have an entire open end whose dominant orientation is in the downstream direction. On some occasions, their upstream end rims were not closed, and they could be eroded by other marks in front of them, for example when an entry furrow developed.

Spiral-furrowed potholes with a spiral rib

On the experimental clay beds, many of the erosional marks had entry spiral ribs (e.g. (Fig. 4D1 to D3) which are widely observed in natural bedrock channels (Alexander, 1932; Ängeby, 1951; Allen, 1982; Jennings, 1983; Baker and Pickup, 1987; Wohl, 1992; Kor and Cowell, 1998; Richardson and Carling, 2005). The spiral rib is a small curved furrow extending in the upstream direction adjacent to the upstream rim of a pothole. The head of the spiral rib was usually cuspate or approximately cuspate and pointed predominantly in the upstream direction. The length and width of the spiral rib was normally far less than the primary pothole with which it was connected. The length of the spiral rib is normally no greater than 1/3 of the diameter of the primary pothole. Sometimes, near the top open rim of potholes, a secondary spiral furrow with a cuspate ridge was present within the pothole (Fig. 4D2).

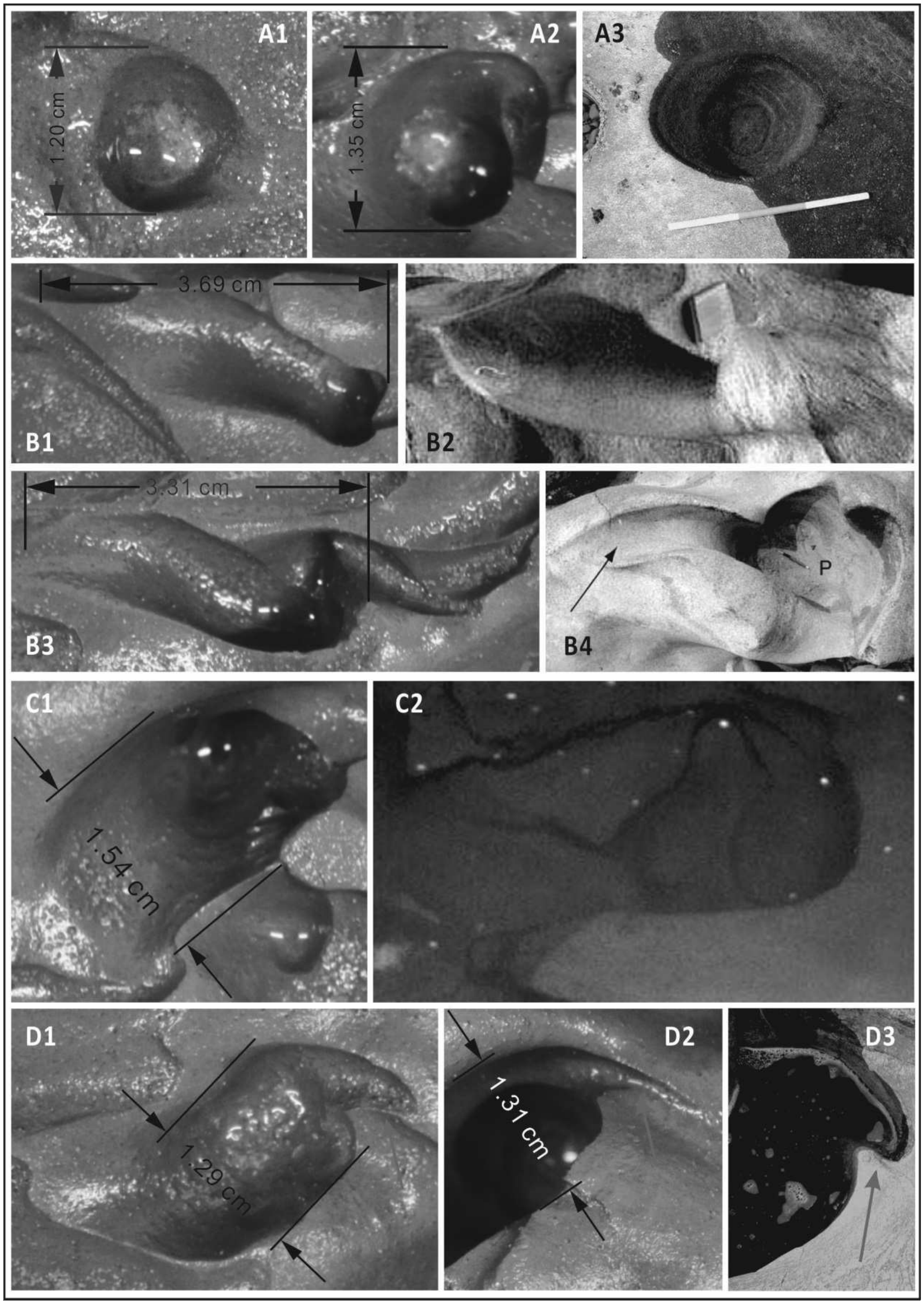

Figure 4. Morphology of potholes in the experiments and in bedrock channels. (1) Simple potholes: A1 and A2 from Exp. 2. A3 shows a simple pothole in fine-grained sandstone from the River Lune (Halton), UK (from Richardson and Carling (2005)). The scale bar in C is 0.6 m long. (2) Potholes with extended exit furrows: The exit furrows of this kind of pothole were

much longer than in potholes with an entry furrow. B1 and B3 from Exp. 2. B2 and B4 are two examples from the field (from Richardson and Carling (2005)). In B2, the notebook is 0.15 m long. B3 and B4 illustrate compound potholes with extended exit furrows. See pen in B4 for scale. (3) Open potholes: C1 from Exp. 2. C2 is from the River Lune (Halton), UK. It is 1.20 m long with a diameter of 0.60 m (from Richardson and Carling (2005)). (4) Spiral-furrowed pothole with a spiral rib: The examples in D1 and D2 were observed in the central part of the bed in Exp. 2. D3 shows a natural example observed in Woolshed Creek, Australia. The pothole is ~1.5 m across in its short dimension (from Richardson and Carling (2005)). The arrow points to the spiral ribs of the potholes in D3. Flow is from right to left. A3, B2, B4, C2 and D3 are reprinted from Richardson and Carling (2005) with permission from GSA.

Longitudinal features

Besides potholes, another principal type of erosional mark in bedrock channels are longitudinal features, commonly flutes and furrows (King, 1927; Allen, 1971; Allen, 1982; Wohl, 1992; Wohl, 1993; Tinkler, 1997; Hancock et al., 1998; Richardson and Carling, 2005). Flutes and furrows are relatively shallow compared with potholes, with their depth usually being much smaller than their length (Richardson and Carling, 2005). In our experiments the average depth of the flutes was 0.82 cm compared with an average depth of 1.93 cm for the potholes (Appendix 1).

Flutes

Flutes are a common form typical of erosive bedforms in bedrock channels (Maxson and Campbell, 1935; Allen, 1971; Tinkler, 1993; Baker and Kale, 1998; Hancock et al., 1998; Whipple et al., 2000b; Richardson and Carling, 2005). The experimental approach herein produced various types of flutes that are almost identical with the flutes present in natural bedrock channels (Fig. 5).

Deep flutes

Deep flutes have been defined as those whose depth is greater than 25% of their length (Richardson and Carling, 2005). Figures 5A1 and A2 show deep flutes in our experimental substrate and natural bedrock, respectively, illustrating they are almost identical with both having a similar internal structure.

Flutes with internal secondary structure

Flutes with an internal secondary structure (Allen, 1971) formed in the experiments and show strong similarities to flutes formed in bedrock substrates (Fig. 5A1 and A2; (Richardson and Carling, 2005)). However, this type of flute was not as common as flutes with external secondary structure in the flume experiments. This may, in part, be because the scale of flutes in the present experiments was too small to contain visible smaller internal secondary structures (Fig. 5B1 and B2).

Flutes with external secondary structure

Most of the flutes in these experiments were classified as flutes with external secondary structures, formed outside the primary flutes (Fig. 5C1 to C5). Previous studies have indicated that flutes with external secondary structures may be caused by a discontinuity in the substrate (Hancock et al., 1998; Richardson and Carling, 2005). However, the clay beds used herein were well mixed and essentially homogenous, and therefore lacked any significant discontinuities. Additionally, the size of these features in the clay bed was variable, with some as large as, or only slightly smaller, than the primary flutes, whilst others were much smaller than the primary flutes. The ratio of the length of the secondary structures and the primary flutes ranges from 0.66 to 0.88 (Fig. 5C1 to C4).

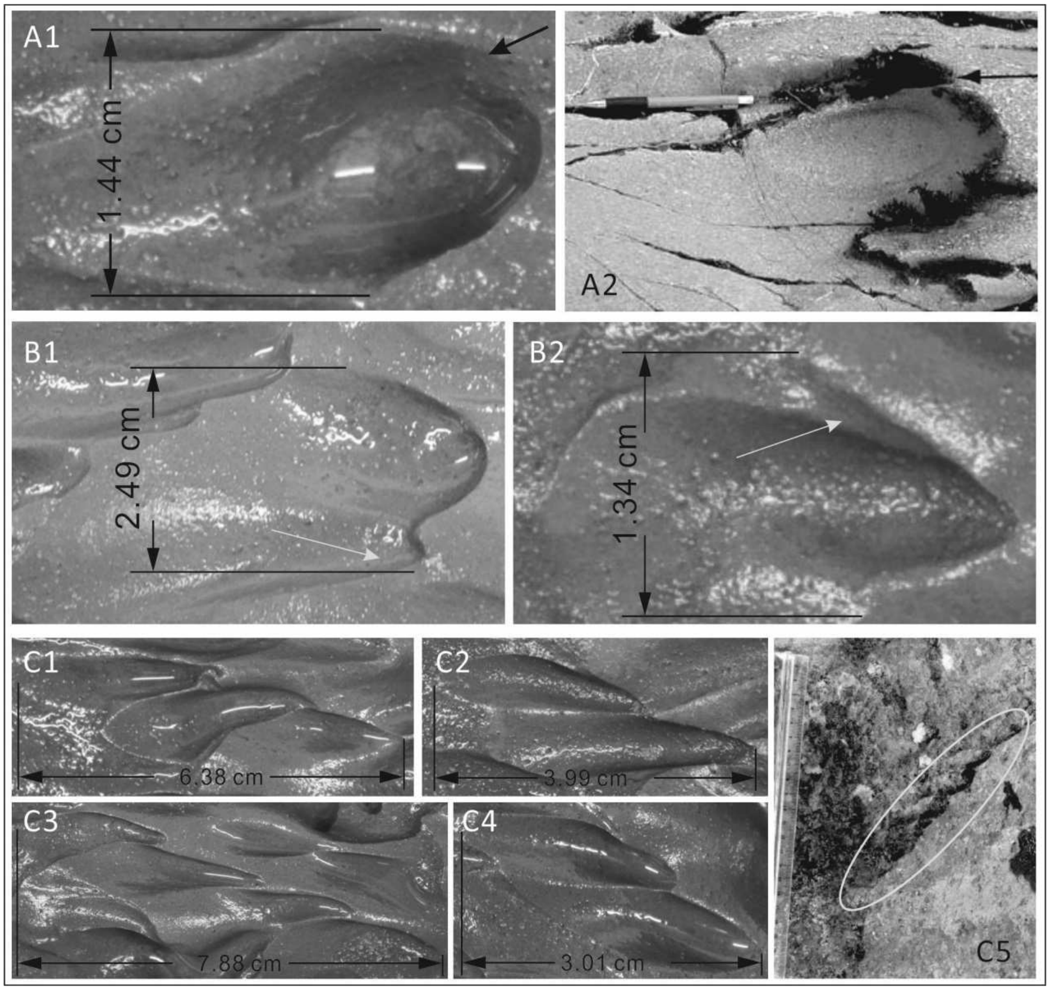

Figure 5. (1) Deep flutes: A1: deep flute in Exp. 1; A2: deep flute in the Borrow Beck, UK (from Richardson and Carling (2005), pen for scale). Both A1 and A2 contain internal secondary flutes close to their upper rims (black arrows). (2) Shallow flutes with internal secondary structure: B1 and B2 show flutes with internal secondary furrows on one side of their flanks, Exp. 2 (arrowed). (3) Flutes with external secondary structures: C1 to C4 demonstrate several rows of flutes developing in Exp. 2. Normally the first flute in a row (the rightmost flute) was regarded as the primary flute, with the remaining flutes defined as secondary. C5 shows a row of small flutes (outlined by ellipse) from the River Dee, UK; ruler in centimetres for scale (from Richardson and Carling (2005)). Flow from right to left in all cases. A2 and C5 are reprinted from Richardson and Carling (2005) with permission from GSA.

Longitudinal furrows

Furrows are also common longitudinal abrasion features in bedrock channels (Fig. 6). According to the definition of a typical furrow, the distal end should be the mirror image of its proximal end (Wohl, 1993; Wohl and Achyuthan, 2002; Richardson and Carling, 2005). The key difference between furrows and flutes is that furrows are almost symmetrical in both cross-sectional and longitudinal profile. The experimental beds demonstrated the development of most types of furrow observed in the field (Fig. 6).

Short furrows usually have closed elliptical rims in plan view (Fig. 6A1 to A4), with their depth being no more than a quarter of their length (Richardson and Carling, 2005). Typically, the average depth of these furrows was 1.37 cm and therefore not as deep as potholes (average depth: 1.93 cm), although potholes are sometimes elliptical in planform. The cross section of a short furrow is a ‘U’ shape, with the inner walls and bottom of the furrow usually being smooth (Richardson and Carling, 2005).

Sinuous parallel-sided furrows

The lengths of sinuous parallel-sided furrows ranged from one (1.29 cm) to more than tens of centimetres (16.22 cm) (Fig. 6B1, B2, B4), with their dominant orientation being longitudinal, with either proximal or distal ends that curved away from the flow direction, and a sinuous furrow. The rims of these furrows were mostly parallel, with their ends being either open or closed, the slope of both ends being gentle, and the rims were either round or cuspate. The walls and the bottom of these furrows were usually smooth without secondary structures or defects. Some long sinuous furrows developed from the connection of curved or sinuous short furrows, and therefore the depth of the furrows was not always uniform. Overall the morphology of these furrows was similar to field examples (Fig. 6B3).

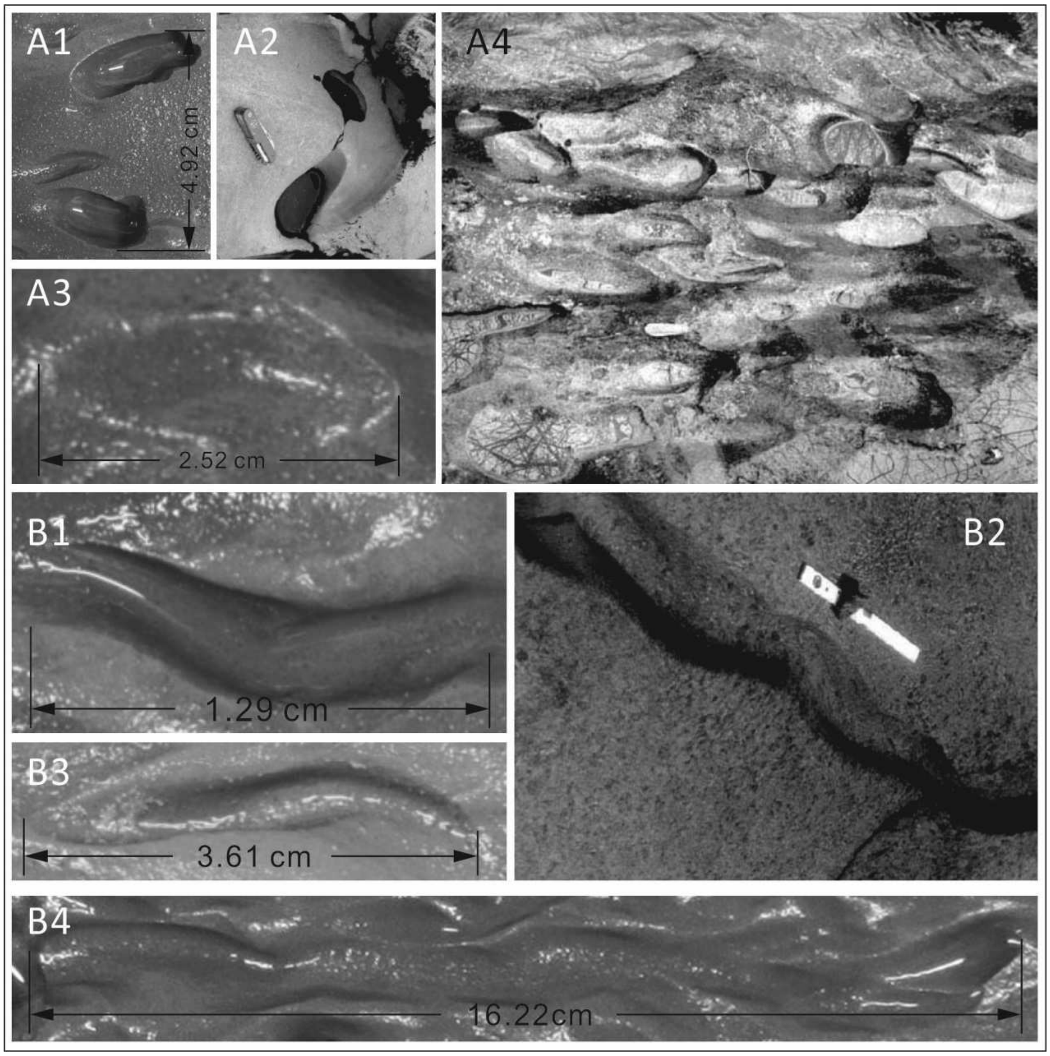

Figure 6. (1) Straight short furrows: A1 and A3 are straight short furrows in Exp. 2. A2 and A4 are field examples from the River Dee, UK; penknife in A2 and A4 (white) for scale (from Richardson and Carling (2005)). (2) Sinuous parallel-sided furrows: B1, B3 and B4: examples of features observed in Exp. 3, 2, and 1 respectively. Flow from right to left. B2 was observed in the River Lune (Halton), UK; the scale is 0.60 m long. Flow from bottom right corner to top left corner. A2, A4 and B2 are reprinted from Richardson and Carling (2005) with permission from GSA.

Convex and undulating surfaces

A number of convex and undulating surfaces also formed in the experiments, with hummocky forms being the most common type within this category (Richardson and Carling, 2005). The most common kind of hummocky form was a sharp-crested hummocky morphology, which resembles ripples and dunes found in cohesionless substrates, but possessed more obvious sharp crests (Fig. 7A1 to A3). This morphology has led to these features being termed pseudo-ripples and pseudo-dunes (Ängeby, 1951; Hancock et al., 1998; Whipple et al., 2000b; Wohl and Achyuthan, 2002; Richardson and Carling, 2005; Hsu et al., 2008).

Sharp-crested hummocky forms

The sharp crests of these features developed non-longitudinally and divided the convex form into two parts, having both a stoss side and a lee side (Fig. 7A1). The slope of the lee side (slope=0.65) was often steeper than that of the stoss side (slope=0.27). In the experiments, the sinuous crests were parallel to each other and the form of the convex parts was similar. The convex forms were arranged in rows with a regular spacing and orientation parallel to the flow direction (Fig. 7A1, A2), thereby producing regular trains of sharp-crested hummocky forms (Richardson and Carling, 2005).

Obstacle marks

Obstacle marks (Fig. 7B1 to B5) are the other typical composite erosional morphology found in the field (Baker, 1974; Lorenc et al., 1994; Richardson and Carling, 2005), and they were also commonly developed on all three experimental beds. In the field, obstacle marks are scour marks caused by flow separation and the horseshoe 'junction' vortex generated when flow encounters projections on the substrate (Simpson, 2001). These obstacle marks possess a crescentic planform shape (Allen, 1982), and in the present experiments they consisted of a raised projection as an obstacle with average width of 0.96 cm and a crescentic reversed furrow (average depth: 1.73 cm) upstream of it. The crescentic reversed furrows were parallel-sided in plan view with either open or closed ends.

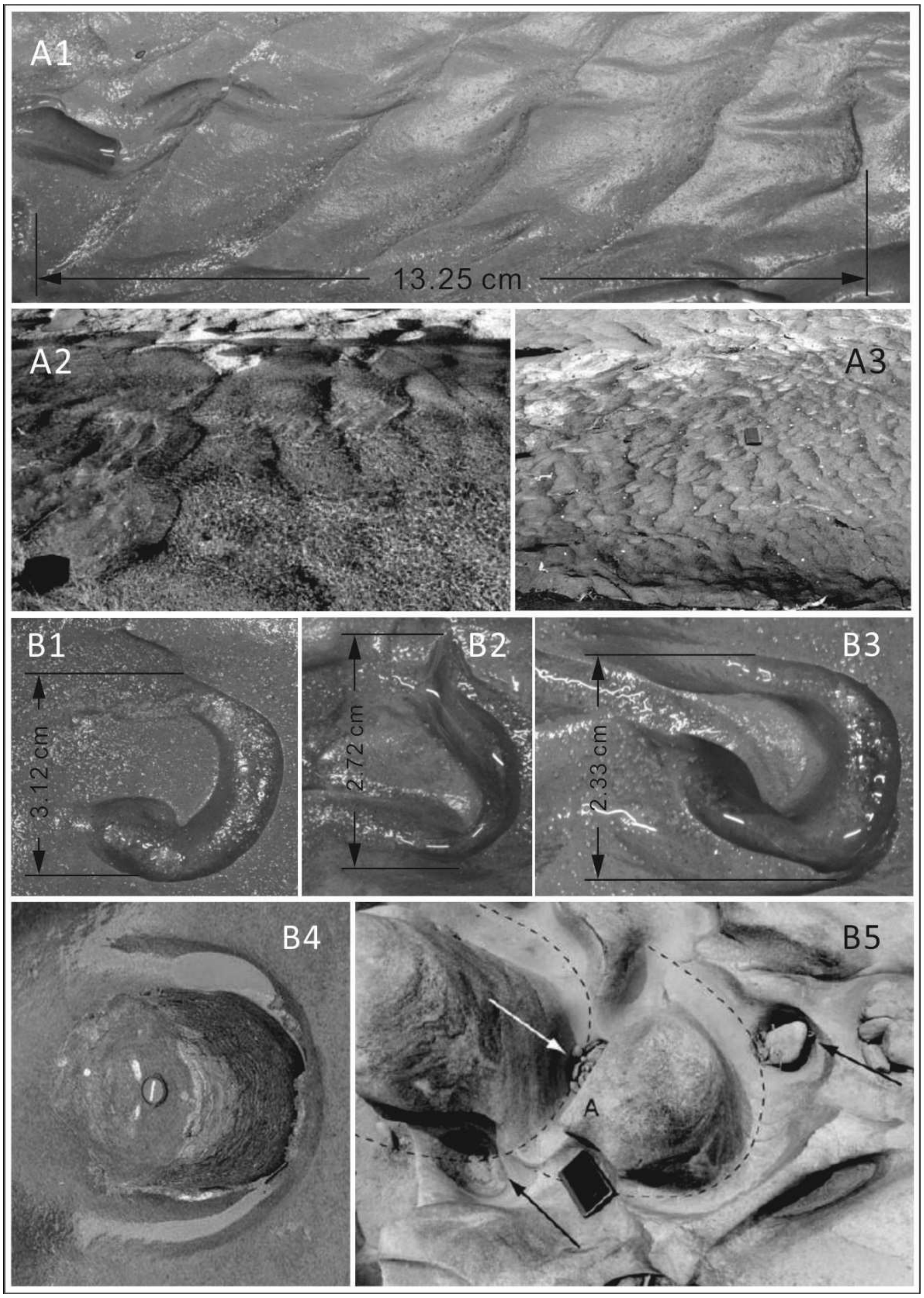

Figure 7. (1) Hummocky forms: A1: Regular trains of sharp-crested hummocky forms observed in Exp. 2. A2 and A3: hummocky forms found in natural bedrock surfaces, camera bag at the bottom left corner of A2, 0.20 m across, and a 0.15 m long handbook in A3, for scale (from Richardson and Carling (2005)). (2) Obstacle marks: B1, B2 are observed in Exp. 1 and B3 are in Exp. 2. B4 and B5: Obstacle marks observed in the field, the lens cap in B4 and the 0.15 m long handbook in B5 for scale (from Richardson and Carling (2005)).

Flow from right to left in all cases. A2, A3, B4 and B5 are reprinted from Richardson and Carling (2005) with permission from GSA.

4. Discussion

The three sediment-laden experiments described herein, using modelling clay with different initial shear strengths, produced a wide array of erosive bedforms that closely replicate many features observed in natural bedrock river substrates, including 7 kinds of potholes, 9 kinds of flutes, 15 kinds of furrows, and 4 examples of other bedforms (Appendix 1). The degree of similarity is so strong that many of the bedforms in the clay were almost identical to examples observed in the field (Figs 4-7). All of the forms were observed to originate on both flat beds and on a bed with initial defects, suggesting that initial bedrock defects are not critical for the genesis of bedforms, or for the overall variety of erosional forms. However, the imposed defects did have a significant effect on altering the specific type of bedform, especially in the genesis of obstacle marks (Fig. 7). The experiments indicated that although obstacle marks also developed on flat beds, they tended to form wherever small hollows were present irrespective of the size and depth of the defects. Whilst the present experiments reproduced the majority of the different bedforms recognised by Richardson and Carling (2005), there are a number of bedforms that were not observed in the current experiments (Appendix 1). Some of these features may be related to heterogeneities in natural substrates that were not present in the experiments. In addition, lateral features were not observed in the present experiments since all experiments utilised a flat bed. If the lack of substrate heterogeneity and lateral topography in the experiments is taken into account, then a remarkable range of forms observed in natural bedrock substrates were observed in the experiments.

Although all three experiments produced similar types of erosional forms, there were some differences in the diversity of forms between the different substrates, with experiment 2 (medium) showing the greatest diversity of forms. In the absence of repeat runs, the degree of variation between runs with nominally identical conditions cannot be quantified. Nonetheless, the present experiments suggest that for the given type of modelling clay, an undrained shear strength of 7.5 kPa, and a shear flow with initial basal shear stress of 4.8 Nm^{-2}, appears to provide the optimal characteristics for an analogue bedrock substrate for creating erosional bedforms.

In the present experiments, erosion is concentrated within the bedforms, widening and deepening them with time, whilst the areas between the bedforms have far less erosion.

The uniform cohesive substrate is unaffected by the plucking process, and similarly dissolution, corrosion and cavitation are not present given the conditions and timescales of the experiments. As a consequence, all erosion is caused by abrasion from the particulate load as confirmed by the initial clear water experiment. The concentration of erosion on the downstream side of bedforms (negative steps) suggests that the abrasion is closely coupled to the flow dynamics, rather than being caused by bed load saltation, in that the latter has been found to erode preferentially the upstream parts of bed protuberances (Whipple et al., 2000a). Calculation of the Rouse number, *Z*:

$$Z = \frac{W_S}{kU_*} \qquad \text{eq. 1}$$

where W_s is the sediment fall velocity, calculated here using the expression of (Gibbs et al., 1971), K is von Karman's constant taken as 0.4, and U_* is the shear velocity, provides an estimation of the transport condition of particles within a flow. For the experiments herein, Rouse numbers, *Z*, were ~0.4-0.6 for the D_{50} of 143 µm and ~1 for the D_{90} of 245 µm, and thus well below the suspension threshold of Z<2.4 (e.g., Lamb et al. (2015)), confirming that even the coarsest material was in suspension.

The present experiments are also the first to reproduce large surfaces composed of arrays of different and varied bedrock bedforms, and in marked contrast to previous experiments that tended to form a narrow range of features prior to formation of a single 'emergent channel' (Shepherd and Schumm, 1974; Wohl and Ikeda, 1997; Finnegan et al., 2007; Johnson and Whipple, 2007; Johnson and Whipple, 2010; Lamb et al., 2015). In part, this may reflect differences in initial conditions. Some previous experiments started with an initial channel (Shepherd and Schumm, 1974; Finnegan et al., 2007), or with the centre being lower than the edges (Johnson and Whipple, 2010), which will both encourage channelization. Other experiments possessed very shallow flow depths (0.02-0.03 m) that may have restricted macroturbulence and bedform development (Wohl and Ikeda, 1997). However, the experiments of Johnson and Whipple (2007) did start with initial planar bed conditions and greater flow depths (0.06-0.09 m), but still produced emergent channel geometries. A major difference between the present experiments and those of Johnson and Whipple (2007) is that the latter experiments were dominated by saltation-driven abrasion, rather than suspension-driven abrasion. This is reflected in Rouse numbers of 18-67 for the D_{50} of 2.5 mm, and 24-90 for the D_{90} of 3.76 mm based on Table 1 from Johnson and Whipple (2007) and calculating fall velocities with Gibbs et al. (1971). Other experiments have largely been undertaken with dominantly saltation-driven abrasion as reflected in their

Rouse numbers, Z ~2.3-6.2, with suspension-dominated abrasion only beginning to occur as narrower channels emerged (Wohl and Ikeda, 1997; Finnegan et al., 2007; Johnson and Whipple, 2007; Johnson and Whipple, 2010). A second important difference is that the present experiments were in the subcritical flow regime, Fr ~0.8, in contrast to previously published experiments that were all strongly supercritical, Fr ~1.4-3.5 (Wohl and Ikeda, 1997; Finnegan et al., 2007; Johnson and Whipple, 2007; Johnson and Whipple, 2010). These previous studies showed that the erosional morphologies are not sensitive to the magnitude of the Fr number, although the Fr numbers in those experiments were greater than that in natural bedrock rivers (Johnson and Whipple, 2007). Our experiments are consistant with those results and demonstrate that even when the flow is subcritical (Fr < 1), erosional bedforms can still be generated by flume-scale experiments with analogue bedrock substrates. Lastly, the present experiments do not exhibit brittle fracturing, unlike those experiments with concrete based or rock substrates or natural bedrock channels (Johnson and Whipple, 2007; Wilson et al., 2013; Lamb et al., 2015), suggesting that brittle fracturing is not important for the genesis of these bedrock features.

Field studies of polished rock surfaces sculpted by erosive bedforms have argued that these surfaces are dominated by suspension- rather than saltation-driven abrasion (Hancock et al., 1998; Whipple et al., 2000a). The present study provides support for these field studies, and provides experimental confirmation of the importance of suspension-driven abrasion in the genesis and maintenance of sculpted surfaces of erosive bedforms.

Some previous experiments have concentrated on the effects of bed load-driven saltation abrasion in order to answer a host of important questions, for example, the effects of varied bed load on the roughness of the bedrock substrate, incision rate and channel morphology (Hancock et al., 1998; Finnegan et al., 2007). Furthermore, the numerical saltation-load abrasion model (Sklar and Dietrich, 2004: Turowski et al., 2007) has been widely utilised to model bedrock river erosion from reach scales, through river profile development, to landscape evolution (e.g., Crosby et al., 2007; Cook et al., 2012; Egholm et al., 2013; Scheingross et al., 2014). However, there is increasing recognition that suspension-load abrasion is also important in many bedrock rivers, and that a total-load model incorporating the effects of abrasion from both saltation-load and suspension-load, is required for more accurate modelling of many of these processes (e.g., Lamb et al., 2008; Scheingross et al., 2014). Despite this recognition that suspension-load is important across a wide range of problems, there are a number of issues with extending existing experimental approaches to the suspension-dominated abrasion regime. Critically, the high tensile strengths of existing substrates coupled to the low angle of impact of suspension driven abrasion, means that large particles are required for any abrasion to occur (>0.2 mm for a range of natural bedrock, even in a ball mill; Sklar and Dietrich, 2001, 2004), and these particles require correspondingly high flow velocities to be transported in the suspension regime. Additionally, even for larger particles erosion rates across existing experimental substrates may be very low, restricting the utility of these substrates due to the large timescales required for measurable erosion. The present experiments demonstrate a method for extending the range of conditions that can be studied experimentally within realistic timescales, to this suspension-driven abrasion regime. The method presented herein thus opens up the potential to examine the temporal evolution of erosive bedrock features, the coupled effects of macroscopic turbulence and bedform development, and the interaction of multiple bedforms. In addition, this experimental approach enables study of the effects of incorporating suspension-load abrasion on landscape evolution, and to the development of total-load abrasion models incorporating suspension-load abrasion.

5. Conclusion

Our experiments produced bedforms highly analogous to natural field examples, and for the first time reproduced the overwhelming majority of bedform types that have been shown to occur on planar surfaces in homogenous substrates. The experiments reported herein confirm field observations that such surfaces and their erosive bedforms are primarily the result of suspension-driven abrasion, rather than bed load driven saltation dominated abrasion. It is also evident that cavitation, dissolution, corrosion, plucking, and supercritical flow conditions are not required for the generation of these forms. Whilst the clay substrates used here do not exhibit brittle fracturing due to discontinuities, experiments were able to reproduce a variety of erosive bedforms. This new method provides a viable approach for extending the physical modelling of saltation driven abrasion, to the suspension-dominated abrasion regime, within realistic laboratory timescales. This approach using modelling clay thus opens up the potential to study the evolution and fluid-bedform coupling of these bedforms, as well as experimentally examine the influence of suspension-dominated abrasion on landscape evolution.

Acknowledgements

This research was supported by Leeds-CSC Scholarship. We are particularly grateful to Gareth Keevil and Russell Dixon at the Sorby Laboratory, University of Leeds, for their extensive help designing and preparing the experimental setup. We would especially like to thank Wayne Stephenson for constructive comments on an early version of this manuscript.

References

Alexander, H.S., 1932. Pothole erosion. The Journal of Geology 40, 305-337.

Allen, J.R.L., 1969. Erosional current marks of weakly cohesive mud beds. Journal of Sedimentary Research 39(2), 607-623.

Allen, J.R.L., 1971. Transverse erosional marks of mud and rock: their physical basis and geological significance. Sedimentary Geology 5(3), 167-385.

Allen, J.R.L., 1982. Sedimentary structures: their character and physical basis, Volume 2. Elsevier Scientific, Amsterdam, pp. 663.

Ängeby, O., 1951. Pothole erosion in recent waterfalls. Lund Studies in Geography, Series A 2, 1-34.

Baker, V.R., 1973. Paleohydrology and sedimentology of the Lake Missoula flooding in eastern Washington. Geol. Soc. Am. Spec. Pap. 144, 1-73.

Baker, V.R., 1974. Erosional forms and processes for the catastrophic Pleistocene Missoula floods in eastern Washington. In: Morisawa, M. (Ed.,) Fluvial Geomorphology, Allen and Unwin, London, 123-148.

Baker, V.R., Kale, V.S., 1998. The role of extreme floods in shaping bedrock channels. In: Tinkler, K.J., Wohl, E.E. (Eds.), Rivers over Rock: Fluvial Processes in Bedrock Channels, American Geophysical Union Geophysical Monograph Series 107, 153-166.

Baker, V.R., Pickup, G., 1987. Flood geomorphology of the Katherine Gorge, Northern Territory, Australia. Geological Society of America Bulletin 98(6), 635-646.

Best, J.L., Kirkbride, A.D., Peakall, J., 2001. Mean flow and turbulence structure of sediment-laden gravity currents: new insights using ultrasonic Doppler velocity profiling. In: McCaffrey, W.D., Kneller, B.C., Peakall, J. (Eds.), Particulate Gravity Currents. International Association of Sedimentology Special Publication 31, Blackwell Science, Oxford, pp. 159–172.

Carling, P.A., Herget, J., Lanz, J.K., Richardson, K., Pacifici, A., 2009. Channel-scale erosional bedforms in bedrock and in loose granular material: Character, processes and implications. In: Burr, D.M., Carling, P.A., Baker, V.R. (Eds.), Megaflooding on Earth and Mars, pp. 13-32.

Carter, C.L., Anderson, R.S., 2006. Fluvial erosion of physically modeled abrasion dominated slot canyons. Geomorphology 81, 89–113.

Cook, K.L., Turowski, J.M., Hovius, N., 2012. A demonstration of the importance of bedload transport for fluvial bedrock erosion and knickpoint propagation. Earth Surface Processes and Landforms, 38, 683–695.

Crosby, B.T., Whipple, K.X., Gasparini, N.M., Wobus, C.W., 2007. Formation of fluvial hanging valleys: Theory and simulation. Journal of Geophysical Research, 112, F3, doi:10.1029/2006jf000566.

Dzulynski, S., 1965. New data on experimental production of sedimentary structures. Journal of Sedimentary Petrology 35, 196-212.

Dzulynski, S., 1996. Erosional and deformational structures in single sedimentary beds: a genetic commentary. Annals Societatis Geologorum Poloniae 66, 101-189.

Dzulynski, S., Sanders, J.E., 1962. Current marks on firm mud bottoms. Trans. of the Connecticut Academy of Arts and Sciences 42, 57-96.

Dzulynski, S., Walton, E.K., 1963. Experimental production of sole marking. Trans. of the Edinburgh Geological Society, 19 279-305.

Egholm, D., Knudsen, M., Sandiford, M., 2013. Lifespan of mountain ranges scaled by feedbacks between landsliding and erosion by rivers. Nature, 498, 475–478.

Elston, E.D., 1917. Potholes: their variety, origin and significance. The Scientific Monthly 5, 554-567.

Elston, E.D., 1918. Potholes: their variety, origin and significance. II. The Scientific Monthly 6, 37-51.

Engel, P., 1976. Impact Wear of Materials. Elsevier Science Ltd, New York, pp 356.

Finnegan, N.J., Sklar, L.S., Fuller, T.K., 2007. Interplay of sediment supply, river incision, and channel morphology revealed by the transient evolution of an experimental bedrock channel. J. Geophys. Res. Earth Surf. 112 (F3), F03S11.

Gibbs, R.J., Matthews, M.D., Link, D.A., 1971. The relationship between sphere size and settling velocity. Journal of Sedimentary Petrology 41, 7-18.

Hancock, G.S., Anderson, R.S., Whipple, K.X., 1998. Beyond power: Bedrock river incision process and form. In: Tinkler, K.J., Wohl, E.E. (Eds.), Rivers over Rock: Fluvial Processes in Bedrock Channels, American Geophysical Union Geophysical Monograph Series 107, 35-60.

Hsu, L., Dietrich, W.E., Sklar, L.S., 2008. Experimental study of bedrock erosion by granular flows. J. Geophys. Res.-Earth Surf. 113, F02001.

Ives, R.L., 1948. Plunge pools, potholes, and related features. Rocks and Minerals 23(1), 3-10.

Jennings, J.N., 1983. Swirlholes and related bedrock river channel forms. The Australian Geographer, 15(6) 411-414.

Johnson, J.P., Whipple, K.X., 2007. Feedbacks between erosion and sediment transport in experimental bedrock channels. Earth Surf. Process. Landf. 32, 1048-1062.

Johnson, J.P., Whipple, K.X., 2010. Evaluating the controls of shear stress, sediment supply, alluvial cover, and channel morphology on experimental bedrock incision rate. Journal of Geophysical Research: Earth Surface 115(F2), F02018.

King, P.B., 1927. Corrosion and Corrasion on Barton Creek, Austin, Texas. The Journal of Geology 35, 631-638.

Kor, P.S.G., Cowell, D.W., 1998. Evidence for catastrophic subglacial meltwater sheetflood events on the Bruce Peninsula, Ontario. Canadian Journal of Earth Sciences 35(10), 1180-1202.

Lamb, M.P., Dietrich, W.E., Sklar, L.S., 2008. A model for fluvial bedrock incision by impacting suspended and bed load sediment. Journal of Geophysical Research, 113, doi:10.1029/2007JF000915.

Lamb, M.P., Finnegan, N.J., Scheingross, J.S., Sklar, L.S., 2015. New insights into the mechanics of fluvial bedrock erosion through flume experiments and theory. Geomorphology, doi: 10.1016/j.geomorph.2015.03.003.

Lamb, M.P., Fonstad, M.A., 2010. Rapid formation of a modern bedrock canyon by a single flood event. Nat. Geosci. 3 (7), 477–481.

Lorenc, M.W., Barco, P.M., Saavedra, J., 1994. The evolution of potholes in granite bedrock, W Spain. Catena 22(4), 265-274.

Maxson, J.H., Campbell, I., 1935. Stream fluting and stream erosion. The Journal of Geology 43, 729-744.

Peakall, J., Ashworth, P., Best, J., 1996. Physical Modelling in Fluvial Geomorphology: Principles, Applications and Unresolved Issues. In: Rhoads, B.L., Thorn, C.E. (Eds.), The Scientific Nature of Geomorphology. John Wiley and Sons, Chichester, 221-253.

Richardson, K., Carling, P.A., 2005. A Typology of Sculpted Forms in Open Bedrock Channels. Geological Society of America Special Paper 392, pp. 108.

Scheingross et al., J.S., Brun, F., Lo, D.Y., Omerdin, K., Lamb, M.P., 2014. Experimental evidence for fluvial bedrock incision by suspended and bedload sediment. Geology, 42, 523-526.

Shepherd, R.G., Schumm, S.A., 1974. Experimental study of river incision. Geol. Soc. Am. Bull. 85, 257–268.

Simpson, R.L. 2001. Junction Flows, Annu. Rev. Fluid Mech., 33, 415–43.

Sklar, L.S., Dietrich, W.E., 2001. Sediment and rock strength controls on river incision into bedrock. Geology 29(12), 1087-1090.

Sklar, L.S., Dietrich, W.E., 2004. A mechanistic model for river incision into bedrock by saltating bed load. Water Resour. Res. 40(6), W06301.

Tinkler, K.J., 1993. Fluvially sculpted rock bedforms in Twenty Mile Creek, Niagara Peninsula, Ontario. Canadian Journal of Earth Sciences 30(5), 945-953.

Tinkler, K.J., 1997. Rockbed wear at a flow convergence zone in Fifteen Mile Creek, Niagara Peninsula, Ontario. The Journal of Geology 105(2), 263-274.

Turowski, J.M., Lague, D., Hovius, N., 2007. Cover effect in bedrock abrasion: A new derivation and its implications for the modeling of bedrock channel morphology. Journal of Geophysical Research, 112, doi:10.1029/2006JF000697.

Whipple, K.X., Hancock, G.S., Anderson, R.S., 2000a. River incision into bedrock: Mechanics and relative efficacy of plucking, abrasion, and cavitation. Geological Society of America Bulletin 112(3), 490-503.

Whipple, K.X., Snyder, N.P., Dollenmayer, K., 2000b. Rates and processes of bedrock incision by the Upper Ukak River since the 1912 Novarupta ash flow in the Valley of Ten Thousand Smokes, Alaska. Geology 28(9), 835-838.

Wilson, A., Lavé, J., 2014. Convergent evolution of abrading flow obstacles: Insights from analogue modelling of fluvial bedrock abrasion by coarse bedload. Geomorphology 208, 207-224.

Wilson, A., Hovius, N., Turowski, J.M., 2013. Upstream-facing convex surfaces: Bedrock bedforms produced by fluvial bedload abrasion. Geomorphology 180-181, 187-204.
Wohl, E.E., 1992. Bedrock benches and boulder bars: Floods in the Burdekin Gorge of Australia. Geological Society of America Bulletin 104(6), 770-778.
Wohl, E.E., 1993. Bedrock channel incision along Piccaninny Creek, Australia. The Journal of Geology 749-761.
Wohl, E.E., 1998. Bedrock channel morphology in relation to erosional processes. In: Tinkler, K.J., Wohl, E.E. (Eds.), Rivers over Rock: Fluvial Processes in Bedrock Channels, American Geophysical Union Geophysical Monograph Series 107, 133-152.
Wohl, E.E., Achyuthan, H., 2002. Substrate influences on incised-channel morphology. The Journal of Geology 110(1), 115-120.
Wohl, E., Ikeda, H., 1997. Experimental simulation of channel incision into a cohesive substrate at varying gradients. Geology 25, 295–298.
Wohl, E.E., Ikeda, H., 1998. Patterns of bedrock channel erosion on the Boso Peninsula, Japan. J. Geol. 106(3), 331-345.
Yin, D., 2013. Genesis and Evolution of Bedforms on Cohesive Mud Beds and Simulated Bedrock Channels. PhD thesis, University of Leeds, UK, pp. 309.
Zen, E., Prestegaard, K.L., 1994. Possible hydraulic significance of two kinds of potholes: Examples from the paleo-Potomac River. Geology 22(1), 47-50.

Appendix

Appendix 1**.** Bedform types and dimensions observed in the present experiments, and comparison with those described by (Richardson and Carling, 2005)**. Remarks indicate which experiment features observed from.**

	Types of bedforms	Rock type	Length (cm)	Width (cm) (lower parts)	Depth (cm)	Remarks
Pothole	Ovoid pothole	Fine-grained sandstone	0.85 1.27	1.20 1.35	1.08 1.61	Fig. 4: A1-Exp. 2 : A2-Exp. 2
	Spiral-furrowed pothole	Microgranite	4.96 2.69	2.92 3.52	2.21 2.45	Exp. 1 Exp. 2
	Incipient pothole	Limestone	-	-	-	-
	Pothole with entry furrow	Calcareous mudstone	2.67 3.96	1.29 1.31	0.96 2.20	Fig. 4: D1-Exp. 2 : D2-Exp. 2

	Pothole with extended exit furrow	Granitic gneiss	3.69 3.31	0.81 1.06	1.60 1.60	Fig. 4: B1-Exp. 2 : B3-Exp. 2
	Open pothole	Fine- grained sandstone	2.41	1.54	2.71	Fig. 4: C1-Exp. 2
	A pothole with horizontal furrows	Calcareous mudstone	-	-	-	-
	Hierarchical pothole	Granitic gneiss	5.03 3.82	4.38 3.03	2.55 2.33	Exp. 1 Exp. 3
	Convoluted pothole	Gneiss	9.46 1.73	5.92 1.25	2.76 1.04	Exp. 1 Exp. 3
	Large isolated breached pothole	Granitic gneiss	-	-	-	-
	Coalesced potholes	Granitic gneiss	-	-	-	-
	Natural arch	Granitic gneiss	-	-	-	-
	Natural pillar	Granitic gneiss	-	-	-	-
	Closed lateral pothole	Granitic gneiss	-	-	-	-
	Lateral pothole	Granitic gneiss	-	-	-	-
	Conjugate linear lateral potholes	Granitic gneiss	-	-	-	-
	Compound lateral pothole of the hierarchical variety	Granitic gneiss	-	-	-	-
	Paired lateral potholes	Dolomit	-	-	-	-
Flute	Broad flute	Limestone	0.94	2.75	0.59	Exp. 2
	Narrow flute	Granitic gneiss	1.56	0.79	0.56	Exp. 2
	Flute with median ridge and internal secondary structures	Calcareous mudstone	2.65	1.47	1.07	Exp. 2
	Spindle-shaped flute	Rhyolitic agglomerate	2.62	0.65	0.59	Exp. 2

	Flute with internal secondary structures	Calcareous mudstone	2.41 3.09 2.71	1.44 2.49 1.34	1.43 0.69 0.47	Fig. 5: A1-Exp. 1 : B1-Exp. 2 : B2-Exp. 2
	Flute with external secondary structures	Limestone	6.38 3.99 7.88 3.01	1.41 1.33 2.44 1.14	0.65 0.84 0.71 1.25	Fig. 5: C1-Exp. 2 : C2-Exp. 2 : C3-Exp. 2 : C4-Exp. 3
	En echelon flutes	Granitic gneiss	4.75	4.15	1.28	Exp. 2
	Paired flutes	Granitic gneiss	2.89	2.07	1.24	Exp. 1
	Lineations	Limestone	8.06	9.01	0.10	Exp. 2
Furrow	Straight short furrow	Limestone	2.09 2.52	0.82 0.80	1.50 0.99	Fig. 6: A1-Exp. 1 : A3-Exp. 2
	Curved short furrow	Calcareous mudstone	2.87	0.63	1.55	Exp. 2
	Cuspate, deep short furrow	Gneiss	2.09 2.52	0.82 0.80	1.50 0.99	Fig. 6: A1-Exp. 1 : A3-Exp. 2
	Paired short furrows	Calcareous mudstone	-	-	-	-
	Short furrow with internal secondary structures	Gneiss	-	-	-	-
	Straight parallel-sided furrow	Fine-grained sandstone	2.81	0.51	1.24	Exp. 2
	Curved parallel-sided furrow	Granitic gneiss	3.91	0.35	1.22	Exp. 2
	Sinuous parallel-sided furrow	Fine-grained sandstone	1.29 3.61 16.22	0.54 0.31 0.90	1.19 1.22 1.90	Fig. 6: B1-Exp. 3 : B3-Exp. 2 : B4-Exp. 1
	Parallel-sided furrow with levees	Fine-grained sandstone	-	-	-	-
	Chute furrow	Limestone	-	-	-	-

Chimney furrow	Interbedded limestone and marl	-	-	-	-
Bifurcating furrows	Microgranite	4.71 23.11	2.68 1.45 (bifurcating point)	1.50 1.50	Exp. 2 Exp. 3
Group of parallel-sided furrows	Limestone	2.20 (average)	0.68 (average)	0.76 (average)	Exp. 2
Regular compound parallel-sided furrows	Andesite	10.24	0.98	1.90	Exp. 2
Irregular compound parallel-sided furrows	Limestone	10.62 10.52	0.37 0.61	1.22 1.34	Exp. 2
Funnel-shaped furrow (underwater)	Medium-grained sandstone	2.44	1.62	0.56	Exp. 2
Bulbous furrow (underwater)	Fine-grained sandstone	3.28	1.55	1.10	Exp. 2
Runnel with cusped margins	Fine-grained sandstone	-	-	-	-
Oblique sloping furrows	Granitic gneiss	-	-	-	-
Compound transverse furrows	Fine-grained sandstone	-	-	-	-
Cross-channel furrow (underwater).	Fine-grained sandstone	-	-	-	-
Straight reversed furrow	Granitic gneiss	-	-	-	-
Curved reversed furrow	Granitic gneiss	4.02	0.61	2.00	Exp. 3
Open-ended reversed furrow	Granitic gneiss	5.79	4.07	2.08	Exp. 1
Branched reversed furrow	Granitic gneiss	-	-	-	-

	Group of parallel reversed furrows	Granitic gneiss	3.28	2.78	1.68	Exp. 1
Convex and undulating surfaces	Convergent furrow complex	Granitic gneiss	6.66	1.96	1.08	Exp. 2
	Yin- yang furrow complex	Calcareous mudstone	-	-	-	-
	Nested curved furrow complex	Medium-grained sandstone	-	-	-	-
	Overhanging concave surface	Granitic gneiss	-	-	-	-
	Cavetto	Limestone	-	-	-	-
	Taffoni	Fine-grained sandstone	-	-	-	-
	Shallow concave surfaces	Calcareous mudstone	-	-	-	-
	Hummocky forms	Limestone	13.25	3.50	0.59	Fig. 7: A1-Exp. 2
	Pseudoripples	Andesite	-	-	-	-
	Microripples	Gneiss	-	-	-	-
	Partially abraded surface	Limestone	-	-	-	-
	Bladed forms	Calcareous mudstone	3.31 7.40	1.93 0.97	0.74 1.60	Exp. 2
	Obstacle mark (Current crescents with secondary sculpting)	Rhyolitic agglomerate	3.12 2.72 2.33	2.38 (0.79) 1.746 (0.47) 2.99 (0.76)	1.84 1.69 1.66	Fig. 7: B1-Exp. 1 : B2-Exp. 1 : B3-Exp. 2
	Pseudoripples with short furrows	Andesite	-	-	-	-
	Runnel with SCHF	Gneiss	-	-	-	-
	Parallel runnels with step-pool structures	Granite	-	-	-	-

High relief Hummocky forms with current crescents	Limestone	-	-	-	-
Hummocky forms with steep lee faces	Limestone	-	-	-	-